https://doi.org/10.5194/egusphere-2026-5480
Preprint. Discussion started: 23 September 2026


# Attributing stratosphere-troposphere mass exchange to tropopause folds: a 45-year trajectory-based climatology and trend analysis in ERA5

Kai-Wei Chang[1] and Chia-Hui Chung[1]

[1]Department of Atmospheric Sciences, Chinese Culture University, Taipei, Taiwan

**Correspondence:** Kai-Wei Chang (zkw2@ulive.pccu.edu.tw)

**Abstract.** Tropopause folds (TF) are one of the main mechanisms of inducing cross-tropopause mass transport, but it is difficult to directly assess the amount of transport due to folds. In this study we perform a multidecadal quantification of stratosphere-to-troposphere (STT) and troposphere-to-stratosphere (TST) mass transport associated with TFs, over the 1980–2024 period using ERA5 reanalysis on model levels. STT and TST events are obtained using trajectory calculations, and the crossing location and time are shown to occur close in time and space with TFs. To quantify the TF-attributed portion of mass exchange, we use the local false discovery rate framework, a method of performing hypothesis testing given a large number of samples, that allows the assignment of a probability to each transport event quantifying likelihood of association to folds. Using this framework we find that globally, 58.3% of STT and 30.1% of TST are fold-associated. Latitudinally resolved analysis shows that the fold-associated transport fraction peaks in the subtropics for both transport types. Trend analysis shows that over the period of 1981–2024 seasonal mean TF frequency has generally increased over the globe, while total STT/TST has generally declined. However, the fold-attributed STT/TST is largely flat, suggesting that the STT/TST decrease is predominantly due to non-fold processes.

## 1 Introduction

Transport and mixing of stratospheric and tropospheric air, i.e. stratosphere-troposphere exchange (STE), influence both atmospheric dynamics and chemistry. One of the primary mechanisms of STE in the mid-latitudes is tropopause folding (Stohl et al., 2003), in which stratospheric air intrudes into the upper and middle, or even the lower troposphere (Holton et al., 1995). These events bring air with high potential vorticity (PV) and ozone concentration downward, possibly into the lower troposphere. Tropopause folds (TFs) are significant contributors to the global tropospheric ozone budget (Fabian and Pruchniewicz, 1977; Roelofs and Lelieveld, 1997) and are linked to local increases of ozone concentration over Asia (Austin and Midgley, 1994; Ding and Wang, 2006; Kumar et al., 2020; Luo et al., 2024), Europe (Akritidis et al., 2016, 2018; Galani et al., 2003; Trickl et al., 2016; Zanis et al., 2014), North America (Bourqui and Trpanier, 2010; Knowland et al., 2017; Kuang et al., 2012, 2017; Langford et al., 2009, 2012, 2018; Lin et al., 2015; Zhang et al., 2014), and southern hemispheric locations including southern Africa (Thompson et al., 2014) and Réunion Island (Liu et al., 2016). Aside from ozone being harmful to humans, Zhang et al. (2024) demonstrated that ozone from stratospheric intrusions is linked to global-scale formation of cloud condensation

https://doi.org/10.5194/egusphere-2026-5480
Preprint. Discussion started: 23 September 2026


nuclei. Based on simulations from the Chemistry-Climate Model Initiative (CCMI) under the Representative Concentration Pathways (RCP) 6.0 scenario, Abalos et al. (2020) suggests that stratospheric ozone in the troposphere is projected to increase by 10–16% by the end of the 21st century, resulting from changes in stratosphere-to-troposphere transport (STT). As TF is one of the primary mechanisms of STE, it is important to characterize its contribution to cross-tropopause mass transport.

While STE in general has been extensively investigated, many studies on fold-driven exchange remain confined to individual case studies. A brief overview of these studies is given below. In contrast, global, multi-decadal assessments of cross-tropopause transport associated with TF events are relatively scarce. In this study, we therefore use the 1980–2024 ERA5 reanalysis (Hersbach et al., 2020) to map fold-associated cross-tropopause mass exchange, examining its spatial patterns, temporal variability, and long-term trends.

The mass flux associated with STE has been quantified by numerous studies, and the estimation methods can be classified as Eulerian and Lagrangian. A commonly adopted Eulerian method is that formulated by Wei (1987), which can estimate the cross-tropopause fluxes separately as components due to diabatic processes, temporal variations of the tropopause "surface", and isentropic mixing. This method has been used to estimate STE in case studies (Lamarque and Hess, 1994; Spaete et al., 1994; Wirth, 1995; Wirth and Egger, 1999) and for global or hemispheric studies (Hoerling et al., 1993; Siegmund et al., 1996), among others. Aside from this method, other Eulerian methods, such as ones based on diagnosis of the potential vorticity budget (Lamarque and Hess, 1994; Gray, 2006) are also demonstrated to be effective.

Lagrangian methods utilize trajectory calculations to estimate mass transport, and various studies used this type of method for global assessments of STE (Bourqui, 2001; Seo and Bowman, 2002; Wernli and Bourqui, 2002; James et al., 2003; Sprenger et al., 2003; Škerlak et al., 2014) and case studies (Bourqui, 2006). When there are multiple tropopauses in a vertical column (as during a fold), the Wei method cannot treat this directly, and this problem is circumvented by taking a single value for the tropopause, such as using the highest altitude or averaging the tropopause height (Gettelman and Sobel, 2000). Though there are problems with both Eulerian and Lagrangian methods, the latter is found generally to be more robust (Gettelman and Sobel, 2000). Also, since the Wei method cannot treat folds directly, the Lagrangian approach is better suited for mass flux estimates in this study.

Lamarque and Hess (1994) conducted a case study of a tropopause folding event over North America and its associated cross-tropopause mass flux, describing the role of diffusion and diabatic effects (including latent heating, cloud-radiation interaction, and radiative heating) on the modification of potential vorticity and how they affect STE. For instance, the cloud-top infrared cooling induced a heating gradient that increased PV above the cloud top, which resulted in the descent of the 2 PVU tropopause and consequently facilitated troposphere-to-stratosphere transport (TST). They find that STT was predominantly due to diabatic effects, and diffusive effects are relatively smaller and tended to facilitate TST in this particular event. Overall, diabatic effects were dominant in the STE process. Wirth (1995), using an idealized model, and Wirth and Egger (1999), in a case study, also reaffirmed the importance of diabatic effects on STT.

Sprenger et al. (2003) quantitatively investigated the relationship between TF and STE. The STE was estimated with the Lagrangian method by Wernli and Bourqui (2002), and the exchange locations (where trajectories cross the tropopause) are matched to fold locations by a spatial and temporal threshold of 300 km and 1 h. It is shown that up to 50–70% of STT and TST

https://doi.org/10.5194/egusphere-2026-5480
Preprint. Discussion started: 23 September 2026


within 20–40° N/S are associated with folds, while in the extratropics it ranges from roughly 0 to 30% (their Figure 8). To the best of our knowledge, this study is the only one that has performed a global study that quantitatively describes the contribution of folds to STE mass exchange. In addition, the results of Sprenger et al. (2003) are based on data from a 1-year period. Though Škerlak et al. (2014) presents a multi-decadal assessment of STE and discusses it in the context of fold occurrences, there is no direct quantification of the relationship between the two. As such, characterization of the variability and trends on the TF-STE connection is needed, and for this reason here we present a quantitative assessment of the relation between TF and STE.

## 2 Data and methods

### 2.1 Trajectory calculations using the ERA5 Reanalysis

ERA5 is the fifth-generation reanalysis from the European Centre for Medium-Range Weather Forecasts (ECMWF), based on the Integrated Forecasting System (IFS) Cy41r2. The native resolution is TL639 (31 $\mathrm{km}$) and 137 hybrid sigma-pressure model levels. All analyses in this study are done using the model-level data on 0.50° × 0.50° grids at 3-hourly intervals.

Lagrangian trajectories are generated with the TRAJ3D model (Bowman, 1993; Seo and Bowman, 2002). The vertical coordinate system is user-specified, and we choose potential temperature $\theta$ for our calculations. Vertical velocity, the potential temperature tendency $\dot{\theta}$, is estimated using

$$\dot{\theta} = Q\frac{\theta}{T} \quad (1)$$

where $Q$ is the temperature tendency, for which we use the ERA5 variable "time-mean temperature tendency due to parametrisations". We use a time step of 30 $\mathrm{min}$ for the trajectory integration, and for ingestion into the TRAJ3D model, horizontal winds and $\dot{\theta}$ are interpolated onto isentropic levels every 10 K between 200 and 400 K, and 20 K between 400 and 600 K. If a trajectory intersects the ground surface, then the trajectory stops at the intersection and its position is not updated going forward in time.

### 2.2 TF 3-D Labeling Algorithm

We use the TF detection algorithm by Škerlak et al. (2015) (S15 hereafter). The algorithm takes PV which we calculate from the ERA5 horizontal winds and temperatures, as well as specific humidity, to find the tropopause as defined by the ±2 PVU surface and perform a 3-D labeling which categorizes the atmosphere into one of five labels as defined in Table 1. To detect folds, the algorithm identifies locations with multiple vertical crossings with the tropopause. Furthermore, for a multiple crossing to be considered a TF, it must pass three criteria that aim to ensure that (1) the TF is connected to the stratospheric air mass, (2) it is not associated with a tropospheric diabatically-produced PV anomaly, and (3) it is not associated with a surface-bound PV anomaly. An example of the algorithm output is shown in Figure 1. Multiple crossings with the tropopause are evident at the grid point detected by the algorithm. The labels given by the algorithm suggest that the fold is considered "stratospheric". The reader is referred to Škerlak et al. (2014) and S15 for a detailed description of the algorithm.

https://doi.org/10.5194/egusphere-2026-5480
Preprint. Discussion started: 23 September 2026


For each grid box with a TF present, the S15 algorithm yields $p_{min}$, the highest tropopause, $p_{max}$, the bottommost extent of the fold, and $p_{mid}$, which is the vertical location of the 2 PVU contour in between $p_{min}$ and $p_{max}$, as shown in Figure 1. S15 uses the depth $\Delta p = p_{mid} - p_{min}$ to categorize folds into shallow $50 \leq \Delta p < 200\,\mathrm{hPa}$, medium $200 \leq \Delta p < 350\,\mathrm{hPa}$, and deep $\Delta p \geq 350\,\mathrm{hPa}$ folds.

| Label | Description |
|---|---|
| 1 | tropospheric (TR) |
| 2 | stratospheric (ST) |
| 3 | stratospheric cutoff or diabatically produced PV anomaly (ST cutoff) |
| 4 | tropospheric cutoff (TR cutoff) |
| 5 | surface-bound cyclonic PV anomaly (Surface-bound) |

**Table 1.** Labels of atmospheric mass designated by the TF detection algorithm by S15.

### 2.3 Lagrangian estimation of STT and TST mass transport

Estimation of cross-tropopause transport in this study closely follows the method developed by Bourqui (2001) and Wernli and Bourqui (2002). The main difference is that while Wernli and Bourqui (2002) spawned trajectories on a longitude-latitude grid, we spawn them at the centers of cells of the quasi-uniform 60 km mesh (obtained at https://mpas-dev.github.io/atmosphere/atmosphere_meshes.html) which has 163,842 cells whose areas range from 2000 to 3200 $\mathrm{km}^2$. Compared to the longitude-latitude grid, which has more densely distributed cells at the poles and a large latitudinal variation in cell area, the quasi-uniform mesh is more even in spacing and area. The procedure is outlined as follows.

1. At every 00Z, we spawn 24 h forward trajectories globally at the centers of 10 hPa layers between 50 and 600 hPa (55 levels from 55 to 595 hPa), and their initial longitude and latitudes are the centers of the quasi-uniform mesh cells. The air mass represented by each air parcel is $\Delta m = g^{-1} A dp$ where $A$ is the cell area of the parcel's origin, $g$ is the standard acceleration of gravity, and $dp = 1000\,\mathrm{Pa}$. Parcel masses range from $2.05 \times 10^{11}$ to $3.28 \times 10^{11}$ kg.

2. Trajectories from the above step that cross the tropopause are labeled as an exchange candidate. These trajectories are extended 120 h backward and forward in time from their initial positions, resulting in a 10-day trajectory.

3. A trajectory is deemed to have undergone cross-tropopause transport if its residence times within the stratosphere and troposphere both exceed a specified threshold. The stratospheric (tropospheric) residence time $\tau_s$ ($\tau_t$) is defined as the continuous time length that the trajectory stays within the stratosphere (troposphere). Figure 2 depicts the concept of $\tau_s$ and $\tau_t$, where in trajectory 2, if $\tau_t$ is too short, then this trajectory only temporarily resides in the troposphere. Designation of a sufficiently long residence time threshold eliminates spurious crossings where an air parcel may have multiple excursions across the tropopause and return into its layer of origin. In this study all STE estimates are based on a residence time of 96 h: a trajectory must remain in its destination layer for at least 96 h after the crossing and in its origin layer for a 96 h period before it, and the crossing is required to occur within the first 24 h after launch.

https://doi.org/10.5194/egusphere-2026-5480
Preprint. Discussion started: 23 September 2026


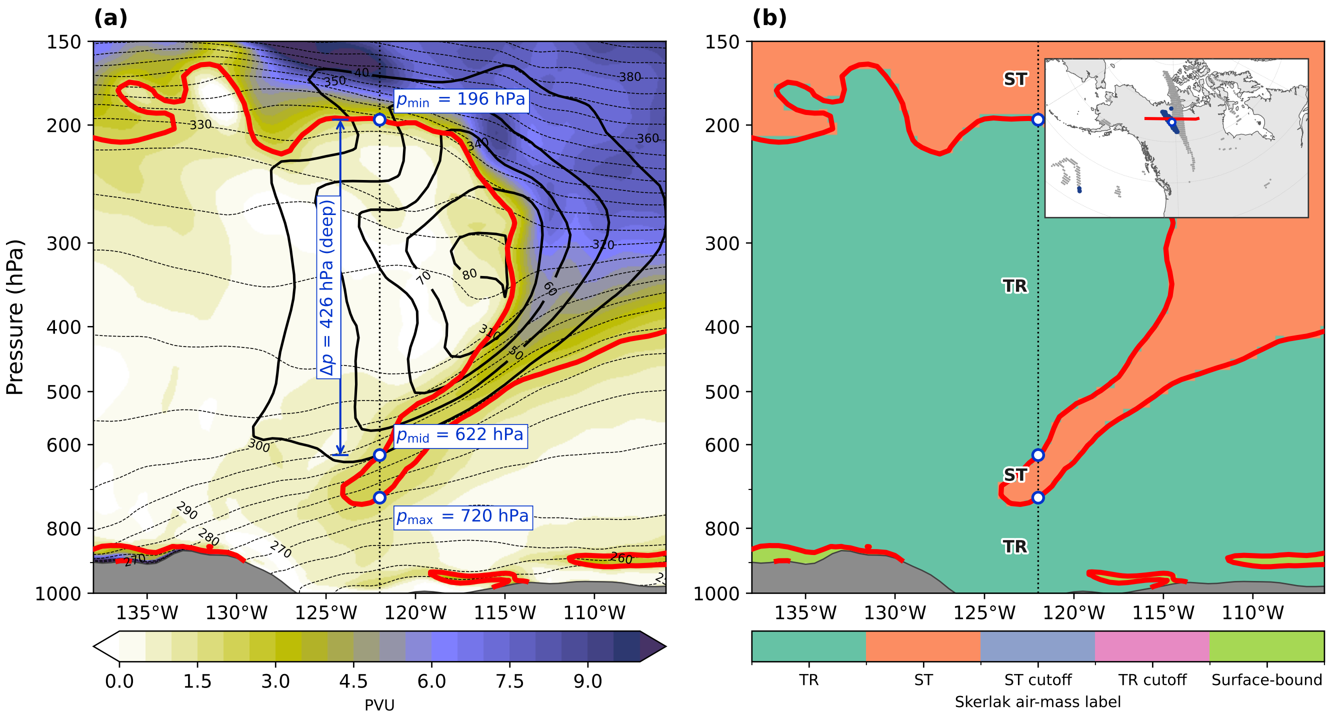


**Figure 1.** Longitude-pressure cross-section of a tropopause fold at 65°N (222–254°E) at 00 UTC 1 Feb 2007. (a) PV (colored shading), potential temperature (dashed contours), absolute wind speed (thick black contours), and 2 PVU tropopause (thick red contours). The dotted vertical line marks the column at 238°E, on which $p_{min}$, $p_{mid}$, and $p_{max}$ (circles) and $\Delta p$ are indicated. (b) Labels assigned by the S15 algorithm, and a map cutout depicting the location of the cross-section (red line) and of the marked column (white dot), and the locations of all detected folds (gray dots) and deep folds (blue dots).

4. For a trajectory that satisfies the above residence time threshold, the cross-tropopause event is taken to occur at point A of trajectory 1 in Figure 2, where the trajectory first leaves its layer of origin. This trajectory undergoes further crossings before finally staying in the troposphere after point B; the residence requirements of the previous step apply to the origin layer before point A and to the destination layer after point B. All mass transport statistics shown hereafter are calculated using the longitude, latitude, and time of point A, taken as the parcel position at the first 3-hourly output time after the crossing. In the following discussions, the terms crossing longitude/latitude/time refer to those properties of point A. Points A and B are the same output time for 84.2% of the exchange trajectories and at most 21 h apart; taking point B instead changes the global integrated seasonal fluxes by at most 0.1%.

5. Trajectories whose crossing latitude is within 10°of the equator are eliminated from the analysis (on the mass flux maps this band is masked), as the 2-PVU tropopause is not suitable there.

https://doi.org/10.5194/egusphere-2026-5480
Preprint. Discussion started: 23 September 2026


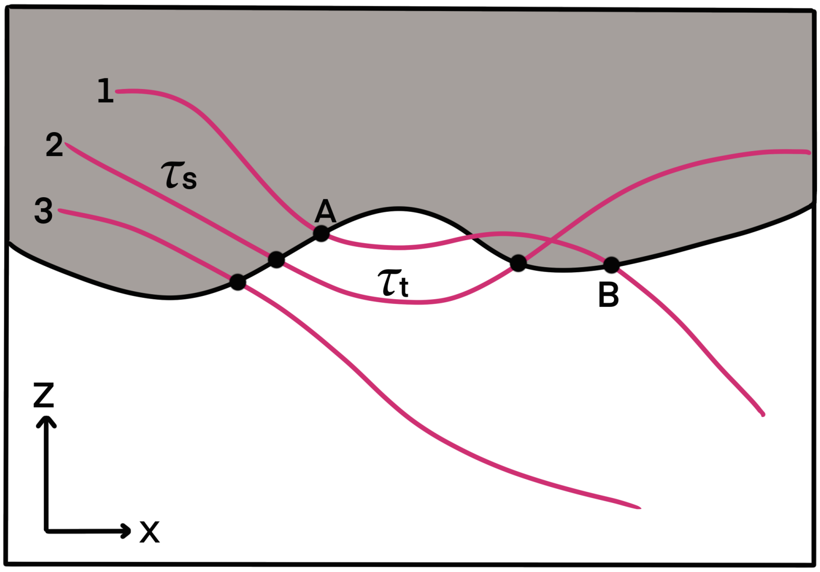


**Figure 2.** Schematic of cross-tropopause trajectories, adapted from Wernli and Bourqui (2002).

6. A final quality control step is performed to eliminate STT trajectories that do not truly originate from the stratosphere. There are rare cases where a parcel had come from air masses of high PV that are of tropospheric origin (e.g. diabatically generated high-PV air), and such cases may wrongly be tagged as STT. Hence, at each 3-hourly position along the 96 h leg on prior to crossing, the trajectory path must be connected to the "stratopsheric reservoir", defined as the air mass with $|PVU| \geq 2$ contiguous up to 10 hPa. Likewise, to ensure TST is transporting into the stratosphere, we verify that in the leg after crossing, TST trajectories must go into the stratospheric reservoir.

We note that among the studies that employ the Lagrangian method based on Wernli and Bourqui (2002), there is significant variation in the residence time thresholds chosen. For instance, while Wernli and Bourqui (2002) uses a threshold of 96 h for their main results, the global assessment of Škerlak et al. (2014) chose 48 h, and a regional case study by Bourqui (2006) used 12 h. Since we aim to highlight the long-lasting transport events, our results are presented using a 96 h threshold.

## 3 Climatology of tropopause folds and cross-tropopause mass fluxes

Hereafter, the term "trajectory" is used to strictly refer to a trajectory that has undergone cross-tropopause transport based on the method described in Section 2.3. To produce maps of STT and TST, the tropopause-crossing locations of the trajectories are binned on 2° × 2° grid boxes, and the mass flux of each trajectory is summed together to calculate seasonal totals of mass fluxes. Figures 3–5 show the seasonal means of STT, TST, and net cross-tropopause mass fluxes, respectively. Overlaid on

https://doi.org/10.5194/egusphere-2026-5480
Preprint. Discussion started: 23 September 2026


these maps are the mean seasonal TF frequencies, defined as the percentage of time steps during which a fold was present at a given grid point during that season.

In the Northern Hemisphere (NH), areas of large STT evidently correspond to the storm tracks in DJF, MAM, and SON. During JJA, relatively strong STT is also found on the northeastern flanks of the Asian Monsoon Anticyclone (AMA; Hoskins and Rodwell, 1995; Siu and Bowman, 2019) and the North American Monsoon Anticyclone (NAMA; Dunkerton, 1995; Siu and Bowman, 2019; Chang et al., 2021). In the Southern Hemisphere (SH), within 30–60°S, the large values of STT extending eastward off the coasts of Australia and South America also correspond to the storm tracks; the location is well matched with areas with high $250\,\mathrm{hPa}$ absolute vorticity variance as shown in Hoskins and Hodges (2005). Overall, STT is highest in midlatitudes and lowest in low latitudes, and the regions of the highest TF frequencies (e.g. along the subtropical jet) do not correspond to the strongest STT regions. In comparison, TST fluxes (Figure 4) are weaker overall, and do not show correspondence to storm tracks. TST, at least visually, seems to align spatially with the pattern of folds in the subtropics. It is noteworthy that in JJA, TST fluxes occur at the northwestern flanks of the AMA and NAMA (whereas STT fluxes are located at the northeastern flank). Both monsoon anticyclones are known to act as efficient conduits of TST (Yan et al., 2019; Clapp et al., 2021), and the northwestern flank of the AMA coincides with the eastern Mediterranean and Middle East region where fold activity has been linked to the Asian summer monsoon (Tyrlis et al., 2014; Wu et al., 2018). Net cross-tropopause fluxes (Figure 5) clearly show a pattern of net downward transport in the midlatitudes and net upward transport in the subtropics. As the subtropical band of high TF frequencies corresponds to the subtropical jet, the patterns show that STT dominates poleward of the subtropical jet.

Table 2 summarizes the 1980–2024 hemispheric and global total fluxes. STT, TST, and net fluxes of the SH are greater in magnitude than those of the NH in all seasons. To assess the consistency of our results with those of previous studies, our estimate of DJF NH net fluxes can be compared to Figure 8 of Gettelman and Sobel (2000), which compiles STE mass fluxes across numerous studies. Our value of $-9.1\times10^{9}\,\mathrm{kg\,s^{-1}}$ across the $2\,\mathrm{PVU}$ surface is reasonable and within the general range of the said figure, though our estimated magnitude is on the smaller side.

## 4 Relationship between tropopause folds and cross-tropopause trajectories

From a physical perspective, if STT or TST is induced by folds, we expect that the path of tropopause-crossing air parcels would have been close in space sometime along their paths before they complete the crossing. It is also expected that the parcels' encounter with TFs should be temporally close to the time of the crossing. In this section we discuss the temporal and spatial relationship between TFs and cross-tropopause trajectories.

Firstly, we examine the vertical location of crossings in relation to folds. For each trajectory, at its crossing location and time we find the nearest grid point with a fold and calculate the horizontal distance between the crossing location and the TF grid point center. The crossing's pressure level $p_{\mathrm{cross}}$ is also recorded, and converted to a fold-relative vertical coordinate

$$\xi=\frac{p_{\mathrm{cross}}-p_{\mathrm{min}}}{p_{\mathrm{max}}-p_{\mathrm{min}}}$$

https://doi.org/10.5194/egusphere-2026-5480
Preprint. Discussion started: 23 September 2026


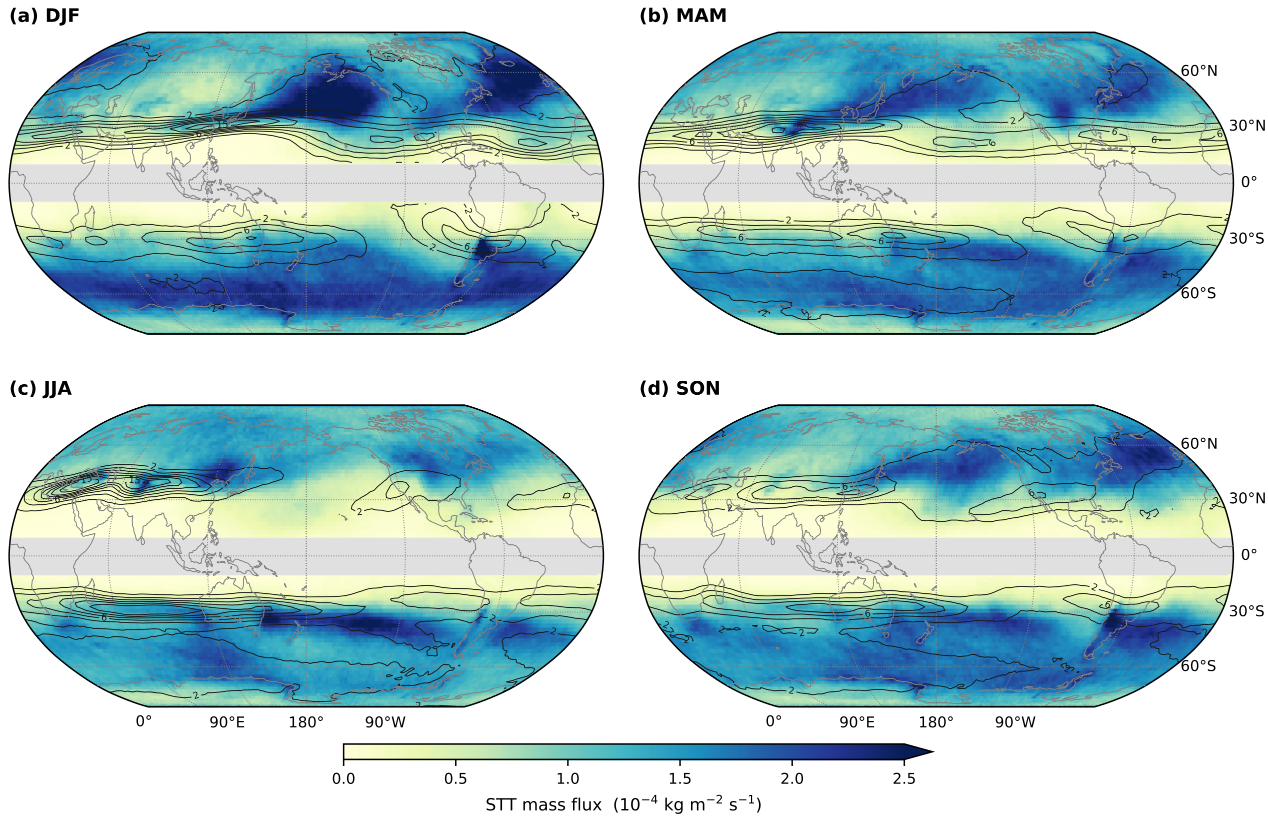


**Figure 3.** The 1980–2024 seasonal mean STT (colors) and TF frequency (in percent; black contours) for (a) DJF, (b) MAM, (c) JJA, and (d) SON. TF frequency is the percentage of 3-hourly time steps with a fold, pooled over the same months and averaged onto the 2° grid; contours are drawn at 2, 4, 6, 8, 10, 12, and 15%, with 2, 6, and 15% labeled. The gray band denotes latitude $|\phi| < 10^\circ$ which is excluded from the analysis. Note that in panel (a), January-February 1980 and December 2024 are included in its calculation.

where $p_{\min}$ and $p_{\max}$ are the minimum and maximum pressure levels of the nearest fold. The density of $\xi$ conditional on the minimum horizontal distance is shown in Figure 6. STT and TST present different features, as STT preferentially occurs at the bottom of the fold near $\xi = 1$, which could be explained as the lowermost portions of folds being eroded and mixed into the troposphere. On the other hand, TST predominantly occurs at the top of the folds, even as the distance is small. Though Lamarque and Hess (1994) described a case study in which TST occurred with transport into the bottom of the fold due to cloud-top diabatic heating/cooling, our results do not find that such processes are dominant at the global scale.

Now we would like to describe the horizontal separation and temporal relation between TFs and trajectories. At every 3 h time step of a trajectory, we can find the distance to the nearest fold. Letting the crossing time be $t = 0$, we bin these distances at various time lags relative to the crossing time, resulting in the density functions of Figure 7 (a) and (d). The observed densities $f_{\text{obs}}$ give a qualitative picture that TF encounters tend to occur before the crossing time, and that the encounters are

https://doi.org/10.5194/egusphere-2026-5480
Preprint. Discussion started: 23 September 2026


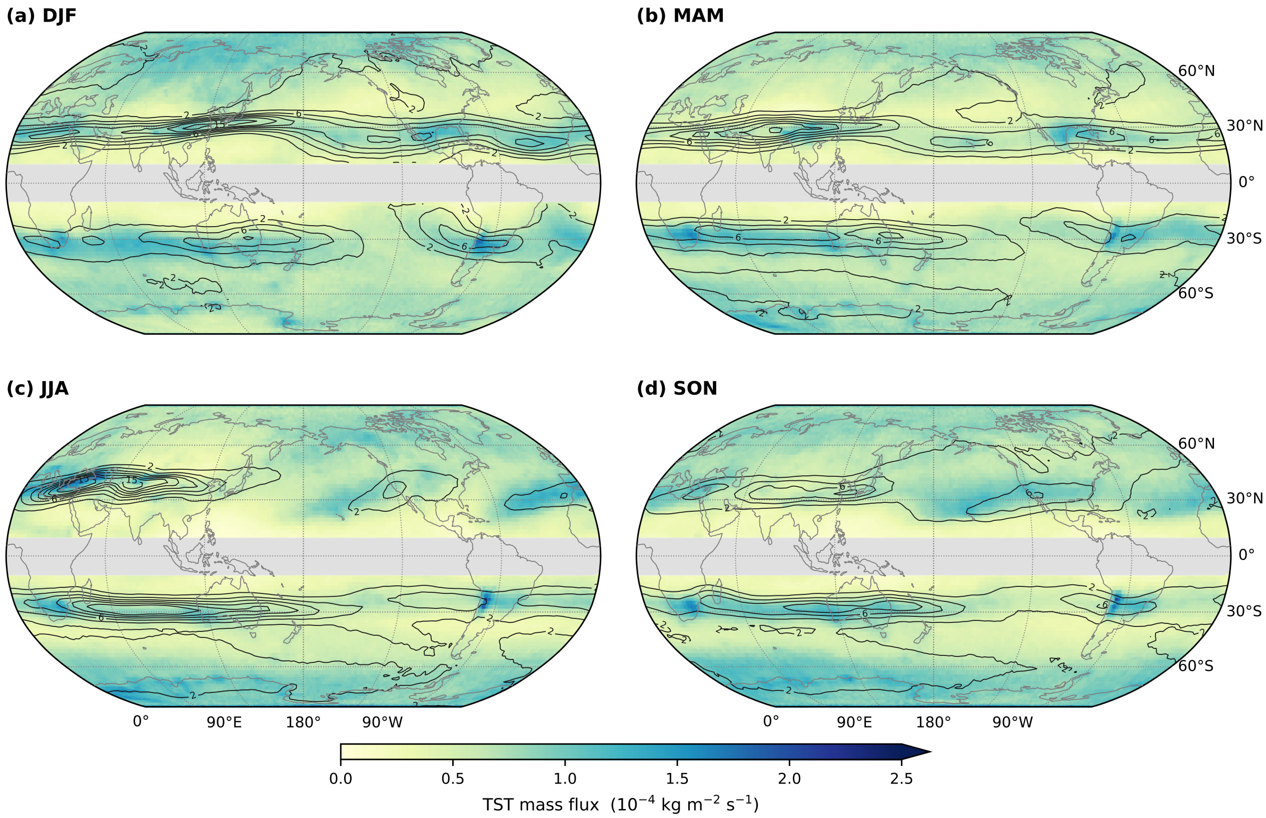


**Figure 4.** Same as Figure 3 except for TST. The colorbar of this panel is the same as that of Figure 3.

horizontally close. To further objectively quantify this relationship, we build a null distribution $f_0(L,d)$ using a time-shifting method that constructs a distribution of time lags $L$ and distances $d$ where TF and cross-tropopause trajectories are unrelated by construction. In plain terms, the method does not modify the trajectories, but replaces the fold field they are compared against with the fold field from the same calendar date and hour in a different year. The procedure is precisely described as follows.

1. Each trajectory is represented by its crossing time $t_c$ (year $y_c$, calendar month, day of month and hour of day), and by its positions $\mathbf{x}(t_c + L)$ at the lags $L = -48, -45, \ldots, +48\,\mathrm{h}$.

2. The six years with available fold detections closest to $y_c$ (excluding $y_c$ itself) are selected to create the null. For example, if the crossing is in 2000, the years 1997, 1998, 1999, 2001, 2002, and 2003 are selected. Near the ends of the record the year pool becomes asymmetric; for instance, a crossing in 1980 draws from years 1981–1986.

3. For each selected year $y'$, let $t'$ be $t_c$ with the year $y_c$ replaced by $y'$, i.e. the same calendar month, day, and hour as the crossing time, but in a different year. At each lag $L$, the distance $d$ between the trajectory position $\mathbf{x}(t_c + L)$ and the nearest fold at time $t' + L$ is recorded.

https://doi.org/10.5194/egusphere-2026-5480
Preprint. Discussion started: 23 September 2026


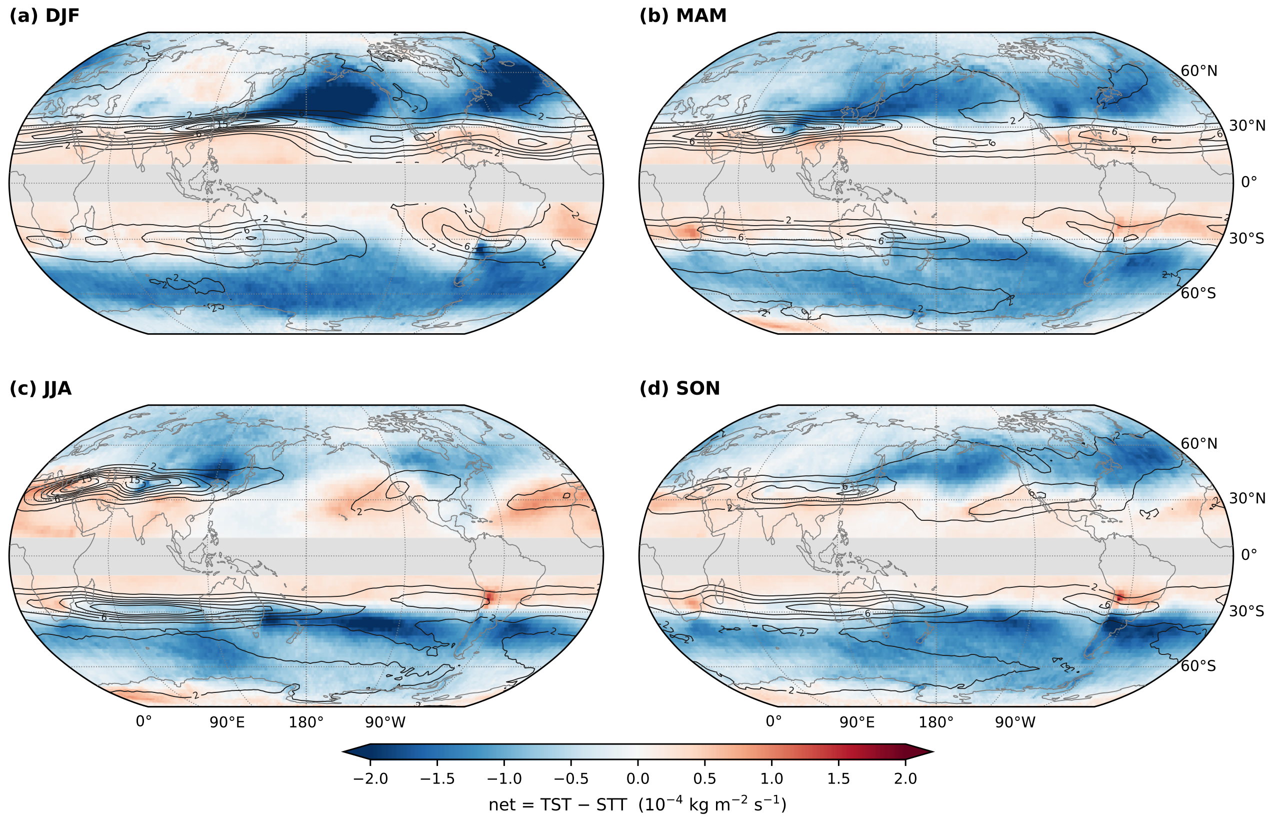


**Figure 5.** Same as Figure 3 except for the net cross-tropopause transport, with positive values indicating net upward transport.

4. Steps 1–3 are performed for all trajectories, and all the $(L, d)$ pairs are binned to produce the null distribution $f_0$.

The resulting null densities are shown in Figure 7 (b) and (e), for STT and TST, respectively. These densities also show decay with increasing distance, but there is no obvious temporal variation. The ratio of the observed and null densities, $r(L, d) = f_{\mathrm{obs}}/f_0$, is shown in Figure 7 (c) and (f), and here values greater than unity indicate that the observed density is greater than the null, meaning that folds are more likely to occur at that time lag and distance than by chance. Roughly speaking, $r$ exceeds unity for $d$ smaller than about 250 km for STT and 320 km for TST near the crossing time. In STT, the highest $r$ aggregates around $L = -3$ h, which is consistent with the physical expectation that folds precondition air parcels for downward transport. TST also shows high $r$ values for negative time lags, but high values persist through a large range of lags (roughly $L \in [-48, -3]$). A possible explanation is that that TST parcels tend to persistently flow along folds (for example along the subtropical jet) before they complete their transport.

https://doi.org/10.5194/egusphere-2026-5480
Preprint. Discussion started: 23 September 2026


**Table 2.** The 1980–2024 annual and seasonal mean STT, TST, and net (TST - STT) cross-tropopause mass fluxes (in $10^9\,\mathrm{kg\,s^{-1}}$) for the Northern Hemisphere, Southern Hemisphere, and globally (excluding |latitude| < 10°). Values in parentheses denote fold-associated percentage of the total fluxes. Note that in the DJF statistics, January-February 1980 and December 2024 are included.

| | | Annual | DJF | MAM | JJA | SON |
|---|---|---|---|---|---|---|
| NH | STT | 19.4 (54.7) | 22.4 (59.5) | 20.6 (54.5) | 15.9 (45.9) | 18.7 (56.6) |
| | TST | 12.8 (25.7) | 13.3 (29.4) | 11.8 (25.5) | 12.7 (21.3) | 13.4 (26.4) |
| | Net | −6.6 | −9.1 | −8.8 | −3.1 | −5.3 |
| SH | STT | 23.8 (61.2) | 24.5 (57.9) | 23.1 (61.6) | 22.8 (63.6) | 24.6 (62.0) |
| | TST | 13.8 (34.2) | 14.3 (33.0) | 14.1 (34.0) | 12.9 (34.9) | 13.7 (35.1) |
| | Net | −10.0 | −10.2 | −9.0 | −9.9 | −10.9 |
| Global | STT | 43.1 (58.3) | 47.0 (58.6) | 43.7 (58.2) | 38.7 (56.4) | 43.3 (59.7) |
| | TST | 26.6 (30.1) | 27.6 (31.2) | 25.9 (30.1) | 25.6 (28.1) | 27.1 (30.8) |
| | Net | −16.6 | −19.3 | −17.9 | −13.1 | −16.1 |

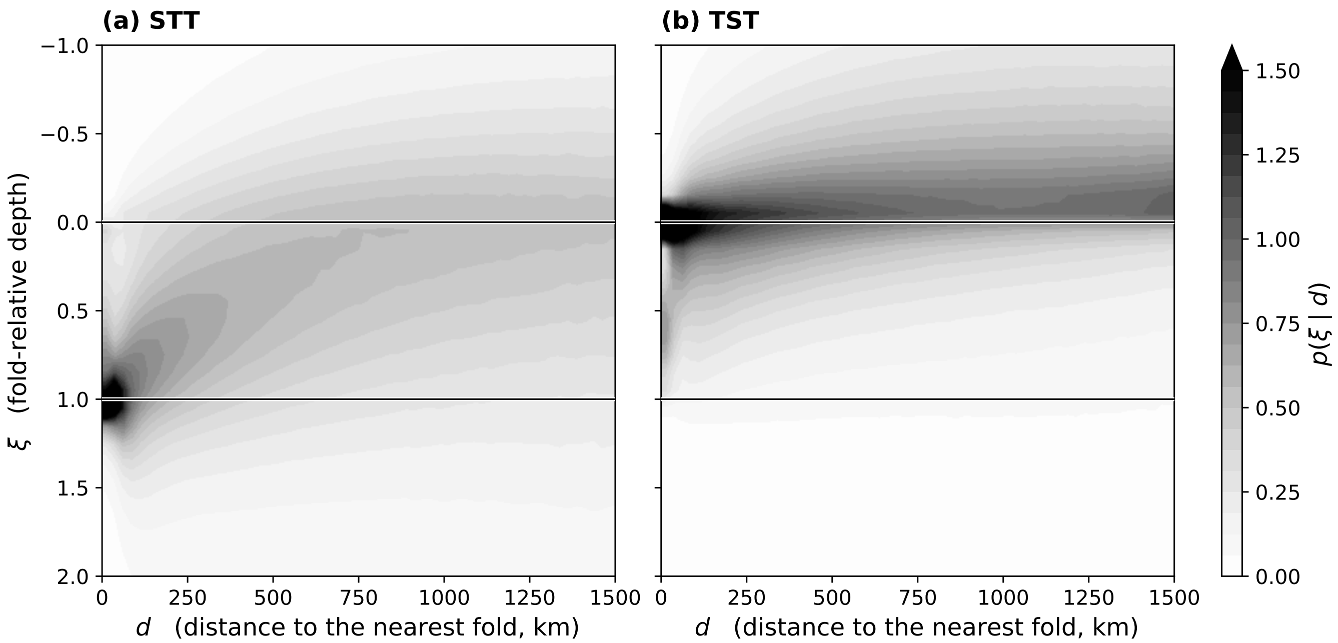


**Figure 6.** Conditional density $p(\xi|d)$ of the fold-relative vertical position $\xi$ of STT (a) and TST (b) crossings, given the distance $d$ to the nearest fold; each distance column is normalized separately. Densities are calculated using all trajectories in 1980–2024.

https://doi.org/10.5194/egusphere-2026-5480
Preprint. Discussion started: 23 September 2026


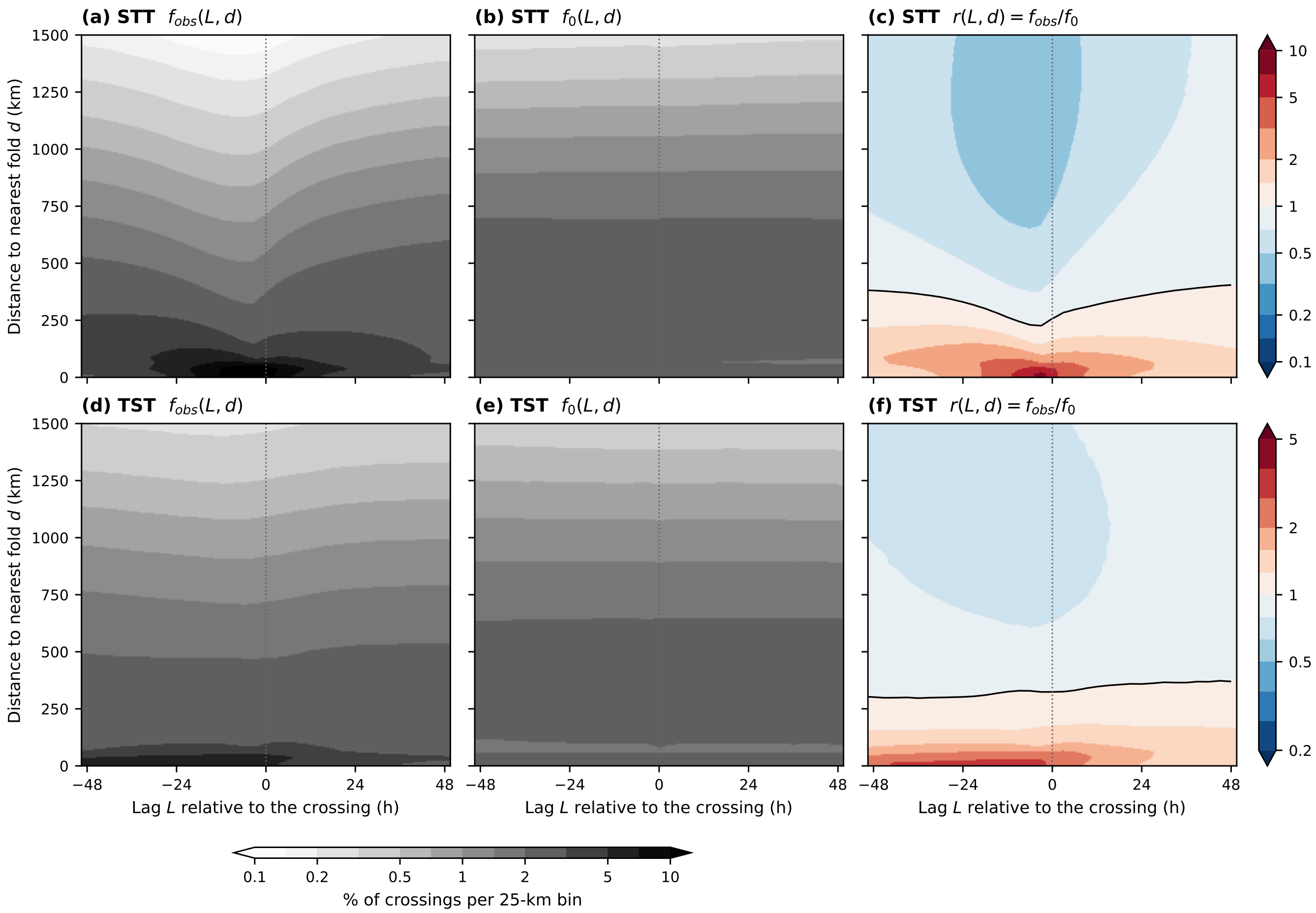


**Figure 7.** Two-dimensional densities of the observed minimum parcel-to-fold distance $d$ at each crossing-relative time lag $L$, calculated using all trajectories from 1980–2024. Panels (a) and (d) show the observed densities for STT and TST respectively, (b) and (e) show the null densities, while (c) and (f) are the ratios of the observed and null densities.

## 5 Quantifying STT/TST attribution to TF using the local false discovery rate

Results of the previous section indicate that cross-tropopause events and TFs exhibit relations in altitude, space, and time. We would like to quantify the amount of mass flux associated with TFs. Sprenger et al. (2003) quantified this based on a fixed matching threshold of 300 km. Figure 7 suggests that this was a reasonable choice, as $r$ falls below one at roughly this distance. However, a fixed threshold equally weights large and small distances, while the latter should be more likely to be truly associated with folds.

To estimate the fraction of mass flux related to TFs we use the framework of local false discovery rate (fdr [1]) (Efron, 2008). The local fdr is an empirical Bayes quantity developed for large-scale simultaneous inference, where thousands of cases are

[1]The acronym is lower-case by convention to distinguish between the global false discovery rate (abbreviated as FDR) from the local one.

https://doi.org/10.5194/egusphere-2026-5480
Preprint. Discussion started: 23 September 2026


tested concurrently to identify those unlikely to belong to the null distribution. This study poses an analogous problem where we have large populations of tropopause-crossing events, among which we want to distinguish events not associated with TFs (null population) from those that are (nonnull population). Since the local fdr yields a quantity that represents the probability that a specific case is null, we can use it to obtain the local true discovery rate, i.e. the probability that a case is non-null. We use this framework to assign a weight $w \in [0,1]$ to each trajectory that quantifies its probability of being nonnull. The method is as follows.

Assume any trajectory to belong to one of the two hidden states: $H = 0$ (unassociated with TF; the null state), and $H = 1$ (associated with TF; the nonnull state). Let $d$ be the nearest parcel-to-fold distance at the time of crossing. The density functions of the null and nonnull trajectory populations are then $f_0(d) = f(d|H = 0)$ and $f_1(d) = f(d|H = 1)$, respectively. The nature of the problem is that $f_1(d)$ is unknown. Let $\pi_1$ be the proportion of nonnull events and $\pi_0$ be that for the null, with $\pi_0 + \pi_1 = 1$. This method assumes the two-mixture model

$$f_{\text{obs}}(d) = \pi_1 f_1(d) + \pi_0 f_0(d) \tag{2}$$

where $f_{\text{obs}}(d)$ is the observed density. Defining the local fdr $\text{lfdr}(d) = P(H = 0|d)$ to represent the probability that a sample belongs to the null case, using Bayes' theorem we can write

$$\begin{aligned} \text{lfdr}(d) &= P(H = 0|d) \qquad (3) \\ &= \frac{P(d|H = 0)P(H = 0)}{P(d)} \\ &= \frac{f_0(d)\pi_0}{f_{\text{obs}}(d)}. \qquad (4) \end{aligned}$$

The quantity $w(d) = 1 - \text{lfdr}(d)$ then represents the probability that a trajectory belongs to the nonnull case. We use this weight to quantify a crossing event's magnitude of association with folds.

To use Equation 4, the estimated observed density $\hat{f}_{\text{obs}}(d)$ is obtained from observed data by simply binning all $d$. The time-shifting method described in Section 4 is used to obtain the estimated null density $\hat{f}_0(d)$. We then use $\hat{f}_{\text{obs}}(d)$ and $\hat{f}_0(d)$ to estimate an upper bound of $\pi_0$ using the inequality below. Starting from Equation 2, we can write

$$f_{\text{obs}}(d) = (1 - \pi_0) f_1(d) + \pi_0 f_0(d). \tag{5}$$

Since by definition $\pi_1 \geq 0$ and $f_1(d) \geq 0$, the first term of Equation 5 is greater than or equal to 0. Hence, $f_{\text{obs}}(d) \geq \pi_0 f_0(d)$, and it follows that

$$\frac{f_{\text{obs}}(d)}{f_0(d)} = r(d) \geq \pi_0 \forall d, \tag{6}$$

so the minimum of $r(d)$ is an upper bound of $\pi_0$, or $\min r(d) \geq \pi_0$. Based on this we calculate the estimated null fraction as $\hat{\pi}_0 = \min r(d)$ for $0 \leq d \leq 1500\,\text{km}$. The bound of $1500\,\text{km}$ is chosen because the densities for larger distances become noisy due to the small number of samples. We can then calculate the estimated nonnull fraction $\hat{\pi}_1 = 1 - \hat{\pi}_0$.

https://doi.org/10.5194/egusphere-2026-5480
Preprint. Discussion started: 23 September 2026


The above framework is applied individually to each 10-degree latitude band, where in each band the observed and null densities $f_{\text{obs}}(d,\phi)$ and $f_0(d,\phi)$, with $\phi$ being latitude, are estimated as in the previous section. The resulting ratios $r(d,\phi) = f_{\text{obs}}(d,\phi)/f_0(d,\phi)$ for STT and TST are shown in Figure 8 (a) and (c) for STT and TST, respectively. Consistent with Figure 7, the ratio is greater than one for distances smaller than roughly 200–300 km for STT and 300–350 km for TST at most latitudes, and out to 400–800 km in the bands closest to the equator. At each latitude band, $\hat{\pi}_0(\phi)$ is estimated by taking the minimum of $r(d,\phi)$ at each latitude, and in Figure 8 (b) and (d) we show the quantity $\hat{\pi}_1(\phi) = 1 - \hat{\pi}_0(\phi)$ which is the estimated lower bound of the nonnull fraction of each latitude band. In the NH (SH), the fraction of TF-associated STT is highest at 30–40 °N (20–30 °S), indicating the strong association of STT to TFs in the subtropics and midlatitudes. The TST nonnull fractions in the NH also maximize at 30–40 °N, but in the SH the high fractions are uniformly spread across 30–60 °S.

The hemispheric nonnull (TF-associated) fractions, obtained as the mass-weighted mean over all crossings in each hemisphere of the trajectory weights $w$ defined below (Equation 7), are presented in the parenthetical values of Table 2. STT nonnull fractions range from 45.9 to 63.6% across all seasons and hemispheres, while TST ranges from 21.3 to 35.1%. Global estimates of the STT and TST nonnull fraction are 58.3% and 30.1%. It can be concluded that STT is significantly more fold-associated than TST.

As we can quantify the association to folds of each trajectory, we can use this framework to obtain the TF-associated mass transport. Let a trajectory's crossing latitude be $\phi_c$ and the crossing point's closest distance to a TF be $d_c$. Generalizing Equation 4 to each latitude band and expressing the local fdr in terms of the density ratio, $\text{lfdr}(d,\phi) = \hat{\pi}_0(\phi)/r(d,\phi)$, the trajectory's weight (association to TF) is

$$w(d_c,\phi_c) = 1 - \frac{\hat{\pi}_0(\phi_c)}{r_{\text{fit}}(d_c,\phi_c)}, \tag{7}$$

where $r_{\text{fit}}(d,\phi)$ is a smooth fit to the values shown in Figure 8 (a) and (c). Because the raw $r(d,\phi)$ estimated from the data is discrete in $\phi$ and in $d$, we perform 1-D binomial P-spline fitting along the $d$ dimension, and piecewise cubic Hermite interpolating polynomial (PCHIP) interpolation in latitude, to build a smooth function $r_{\text{fit}}(d,\phi)$. The resulting $r_{\text{fit}}(d,\phi)$ is shown in Figures S1 and S2, while the resulting weight function $w(d,\phi)$ is shown in Figure S3. Trajectories with no fold within 1500 km are assigned $w = 0$. Given a trajectory's mass $\Delta m$, its TF-associated transport is then $w(d_c,\phi_c)\Delta m$. This quantity is summed over all trajectories within 2° × 2° grid boxes to produce the TF-associated flux maps in Figures 9 and 10.

Overall, the patterns of TF-associated STT and TST are similar to those of the total transport. TF-associated fractions of STT in the NH storm tracks range from roughly 0.6 to 0.7 during DJF, MAM, and SON. Interestingly, the fraction over the mid-to-high latitudes of Eurasia is lower than over the storm tracks, but the reason requires further investigation. As for TST, the highest TF-associated fractions are close to the subtropics near 30° N/S.

## 6 Trends of TF, total STE, and TF-associated STE

Seasonal trends in TF over 1981–2024 (Figure 11; 44 years per season) are estimated with the Theil–Sen estimator (Sen, 1968) and tested per grid point with the two-sided Mann–Kendall test (Mann, 1945; Kendall, 1975). As suggested by Wilks (2016),

https://doi.org/10.5194/egusphere-2026-5480
Preprint. Discussion started: 23 September 2026


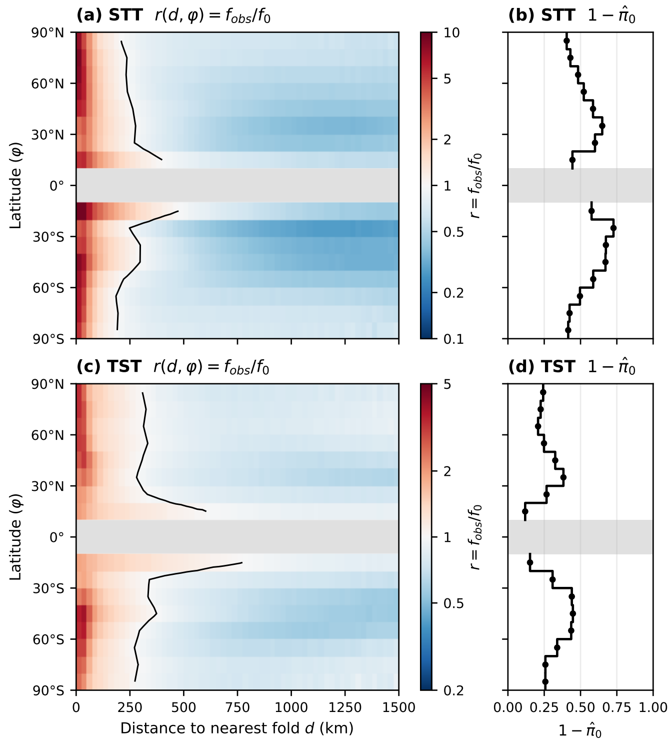


**Figure 8.** Values of the ratio between the observed and null densities, $r(d, \phi)$, as defined in Equation 6 for (a) STT and (c) TST, stratified by 10-degree latitude bins. Panels (b) and (d) show the estimated nonnull fraction of each latitude $\hat{\pi}_1(\phi) = 1 - \hat{\pi}_0(\phi)$ where $\hat{\pi}_0(\phi) = \min(r(d, \phi))$ at each latitude $\phi$.

significance is controlled for multiplicity with the Benjamini–Hochberg false-discovery-rate (FDR) procedure (Benjamini and Hochberg, 1995), applied separately to each map at $\alpha_{\text{FDR}} = 0.10$. Throughout, $\alpha_{\text{FDR}}$ denotes the nominal level at which the false discovery rate of a family of tests is controlled, a test being declared significant when its Benjamini–Hochberg-adjusted $p$ value does not exceed $\alpha_{\text{FDR}}$; the family differs between figures and is stated in each caption. The procedure is conservative under spatial correlation, so $\alpha_{\text{FDR}} = 0.10$ corresponds to an effective global test level of about 0.05 (Wilks, 2016). Hatching therefore marks gridpoints passing the FDR criterion. Lin et al. (2024) evaluated trends by applying the S15 TF algorithm on the ERA5 product on 37 pressure levels, and their trend maps are similar to ours although the results here contain significantly more negative slopes of larger magnitude. In DJF, areas near high latitudes show significant positive trends, as well as some spots near South America and Australia. In MAM, large positive slopes are found along the subtropical bands of both hemispheres, though they do not pass the significance test. In JJA, parts of the positive trends around the AMA region are significant, and positive trends are found at the South Pole. In SON, significant trends are mostly near the poles. As studies on TF trends are relatively scarce, more study is needed to evaluate the presence and mechanism of these trends.

https://doi.org/10.5194/egusphere-2026-5480
Preprint. Discussion started: 23 September 2026


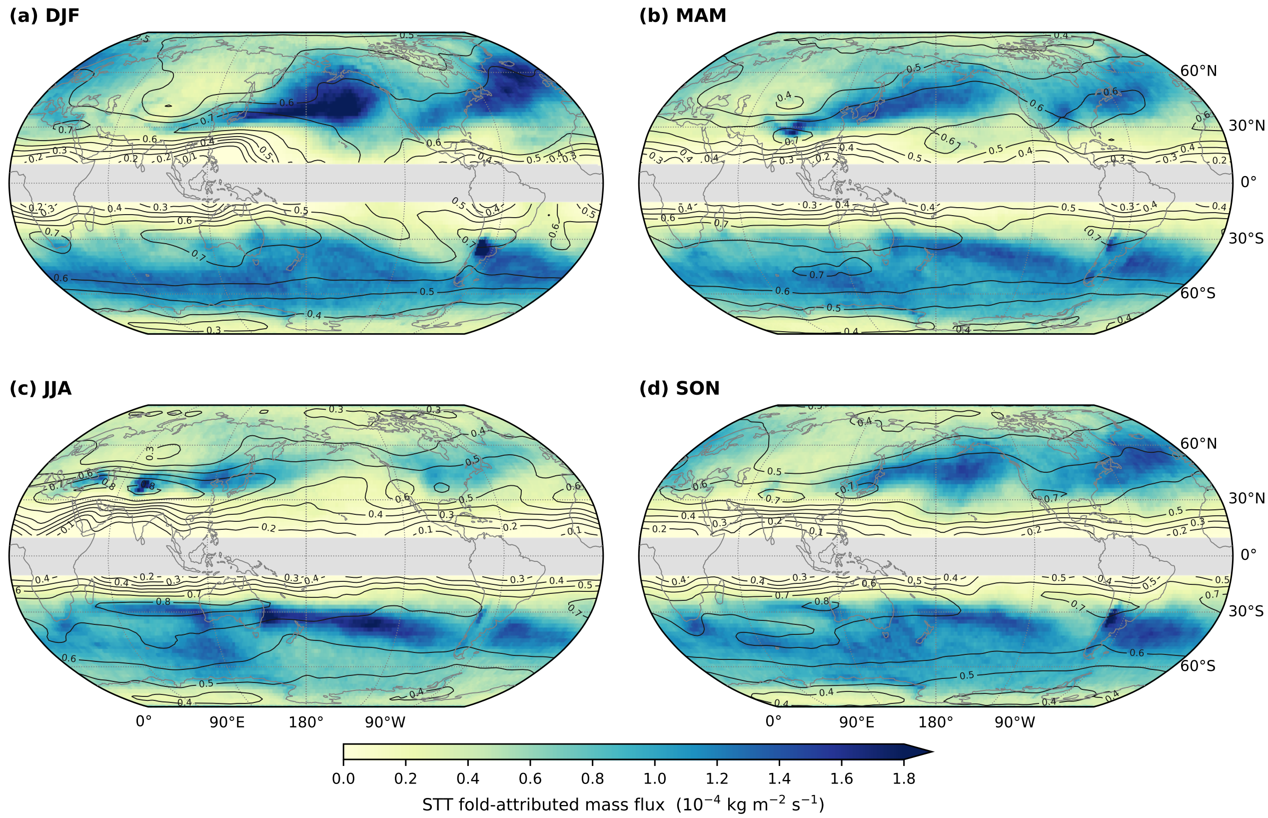


**Figure 9.** The 1980–2024 seasonal mean of TF-associated STT mass fluxes (colors) for (a) DJF, (b) MAM, (c) JJA, and (d) SON. Black contours show the fraction of total STT that is TF-associated. Note that in panel (a), January-February 1980 and December 2024 are included in its calculation.

Global and hemispheric TF trends are shown in Figure 12. Here the TF frequency is a cosine-latitude weighted mean over $|\phi| \geq 10°$, expressed as a percentage of the base area (NH/SH: area of 10°–90°N/S; global: sum of NH/SH area). The slope is estimated by the Theil–Sen estimator and significance is assessed with a moving-block resampling test (Kunsch, 1989; Wilks, 1997) with a block length of 6 years. Blocks are permuted rather than drawn with replacement, so the null series retain the sample's marginal distribution. The resulting $p$ values are controlled for multiplicity with the Benjamini–Hochberg procedure at $\alpha_{\mathrm{FDR}} = 0.10$ over the four seasons of each region. Aside from the NH in DJF and MAM, all other seasons and areas have significant positive trends.

Figure 13 shows trend maps of seasonal mean TST fluxes. Statistical testing is done in the same way as for Figure 11. From Figure 13 it is apparent that most of the significant trends are negative, suggesting decreases in TST fluxes over the study period. The same figure for STT is relegated to the supplementary material (Figure S4) because practically no region carries statistical significance.

https://doi.org/10.5194/egusphere-2026-5480
Preprint. Discussion started: 23 September 2026


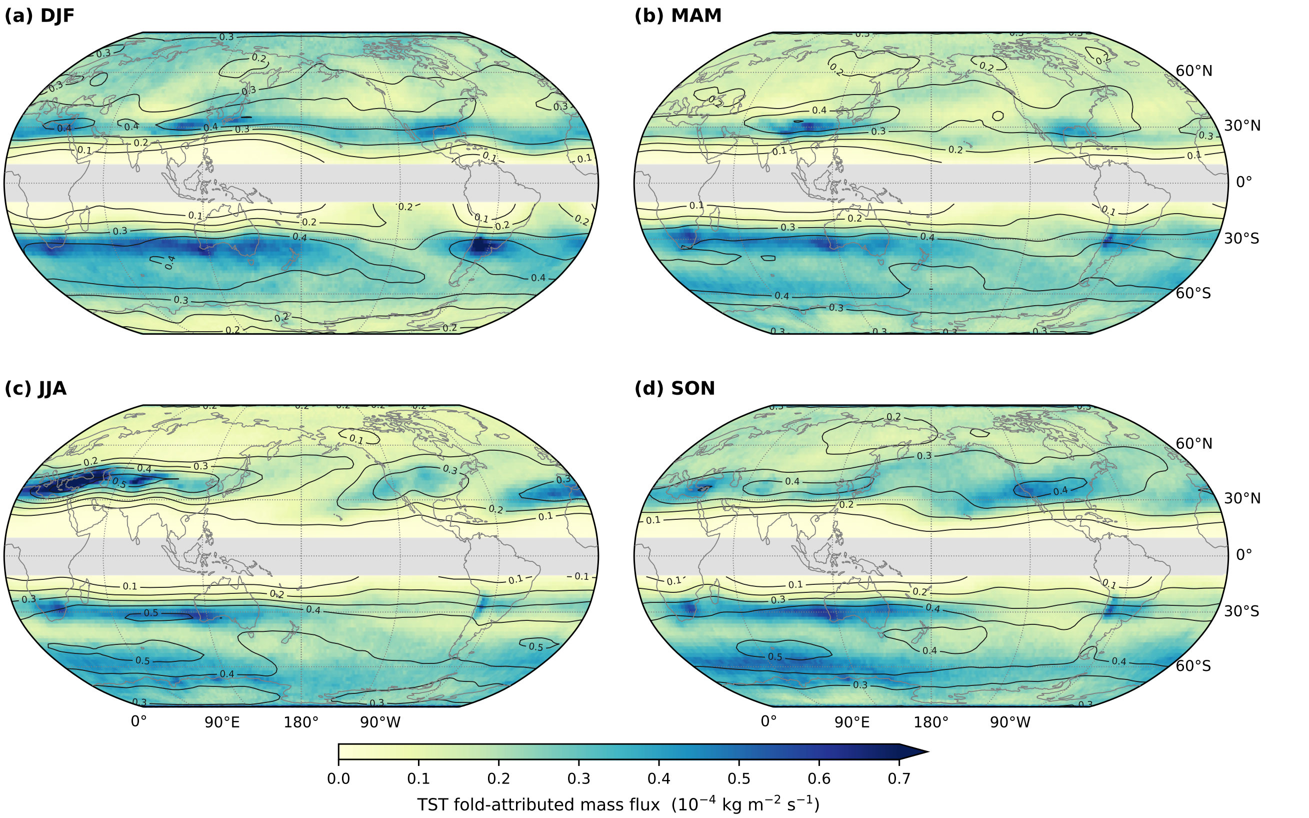


**Figure 10.** Same as Figure 9 except for TST (note that the colorbar ranges are different between the two figures).

Global and hemispheric total STT/TST flux trends (top row of Figures 14 and 15 respectively; tested as for Figure 12) show that in all seasons the STT trends are significantly negative in the SH, while none are in the NH. This suggests that the negative global STT trends are predominantly due to the SH. The middle rows of these two figures are the fold-attributed fluxes, and only three cases (STT: MAM SH and JJA NH; TST: JJA NH) have significant trends while all others are relatively flat over the study period. Combined with the decreasing trends of total STT/TST fluxes, this results in positive trends of fold share (third row of these two figures) that are significant in all seasons and hemispheres. Equivalently, the decline in total STT/TST is largely due to the non-fold-associated component; in some seasons the fold-attributed flux is flat or even trends weakly upward while the total falls. A plausible hypothesis is that transport mechanisms such as transport due to large-scale ascent/subsidence, Rossby wave breaking, or other processes could be declining, but this requires further study.

Finally, we present the trends of annual-mean TF frequency, total STT/TST fluxes, and fold-attributed fluxes in Figure 16. Unlike the seasonal TF trend maps, the annual mean (Figure 16a) exhibits significant trends not only in high latitudes but also in the subtropics, with the majority of significant trends being positive. The annual mean total STT also now shows areas of significant negative flux trends (for instance over the South Pacific Ocean), and sporadic spots of positive trends over the North

https://doi.org/10.5194/egusphere-2026-5480
Preprint. Discussion started: 23 September 2026


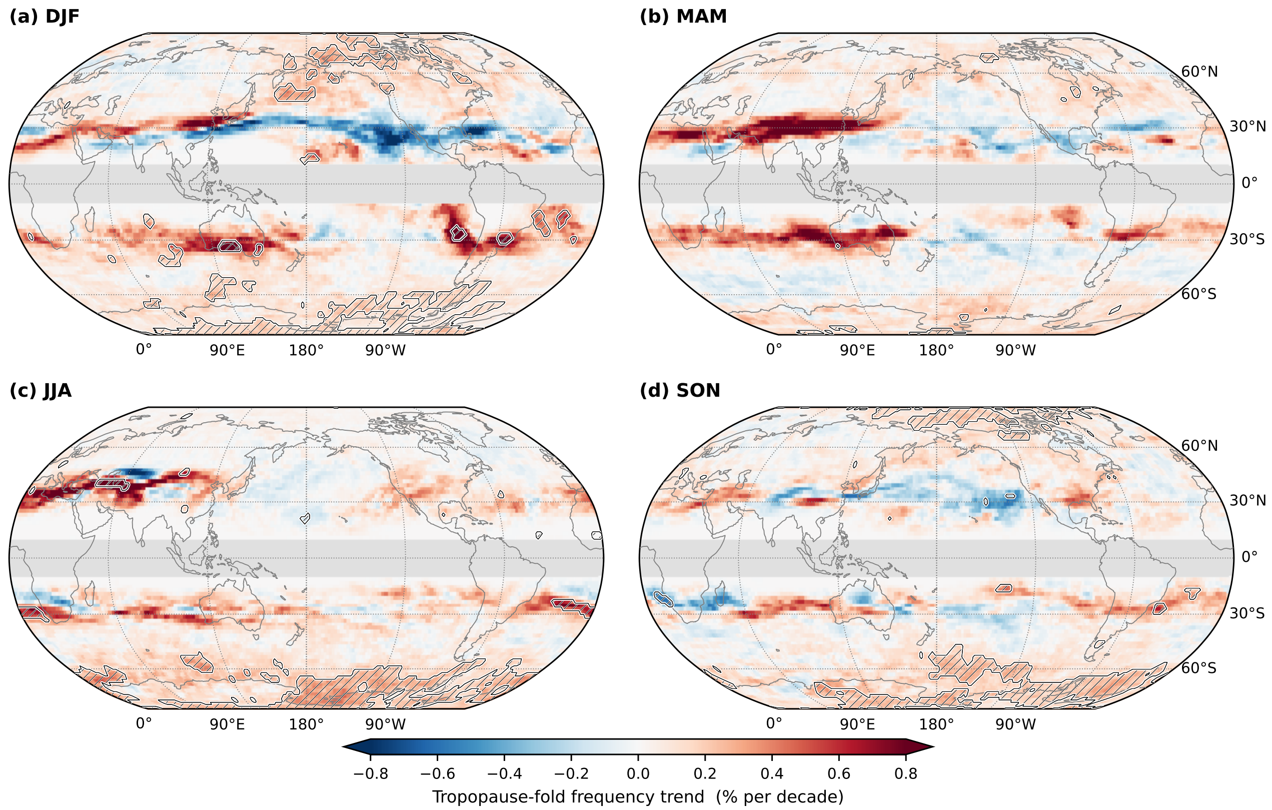


**Figure 11.** TF trends (colors, percent per decade) over 1981–2024 for (a) DJF, (b) MAM, (c) JJA, and (d) SON. Trends are computed on a 2° grid, onto which each season's frequency field is averaged before the trend is estimated. Hatched regions pass the Benjamini–Hochberg FDR criterion at $\alpha_{\mathrm{FDR}} = 0.10$.

Pacific and North America. Annual mean total TST shows large swaths of decreasing fluxes from low to middle latitudes. Figure 16b and c may be compared to Figure 13 of Škerlak et al. (2014) which shows the mass flux trends from 1979 to 2011. The spatial patterns and magnitudes are largely comparable, and they also find relatively strong positive trends of STT over North America and negative trends in TST at the southern tip of South America. The spatial patterns of the fold-attributed flux trends (Figure 16d and e) largely resemble that of the total fluxes, though the areas of significant trends are smaller.

## 7 Conclusions

By using ERA5 data from 1980–2024, this work investigates the relationship between TF and cross-tropopause mass transport estimated through the Lagrangian method, i.e. using parcel trajectory calculations. By examining the trajectory paths in relation to the time and location of TF events, we establish that both TST and STT occur close in time and space relative to folds. It

https://doi.org/10.5194/egusphere-2026-5480
Preprint. Discussion started: 23 September 2026


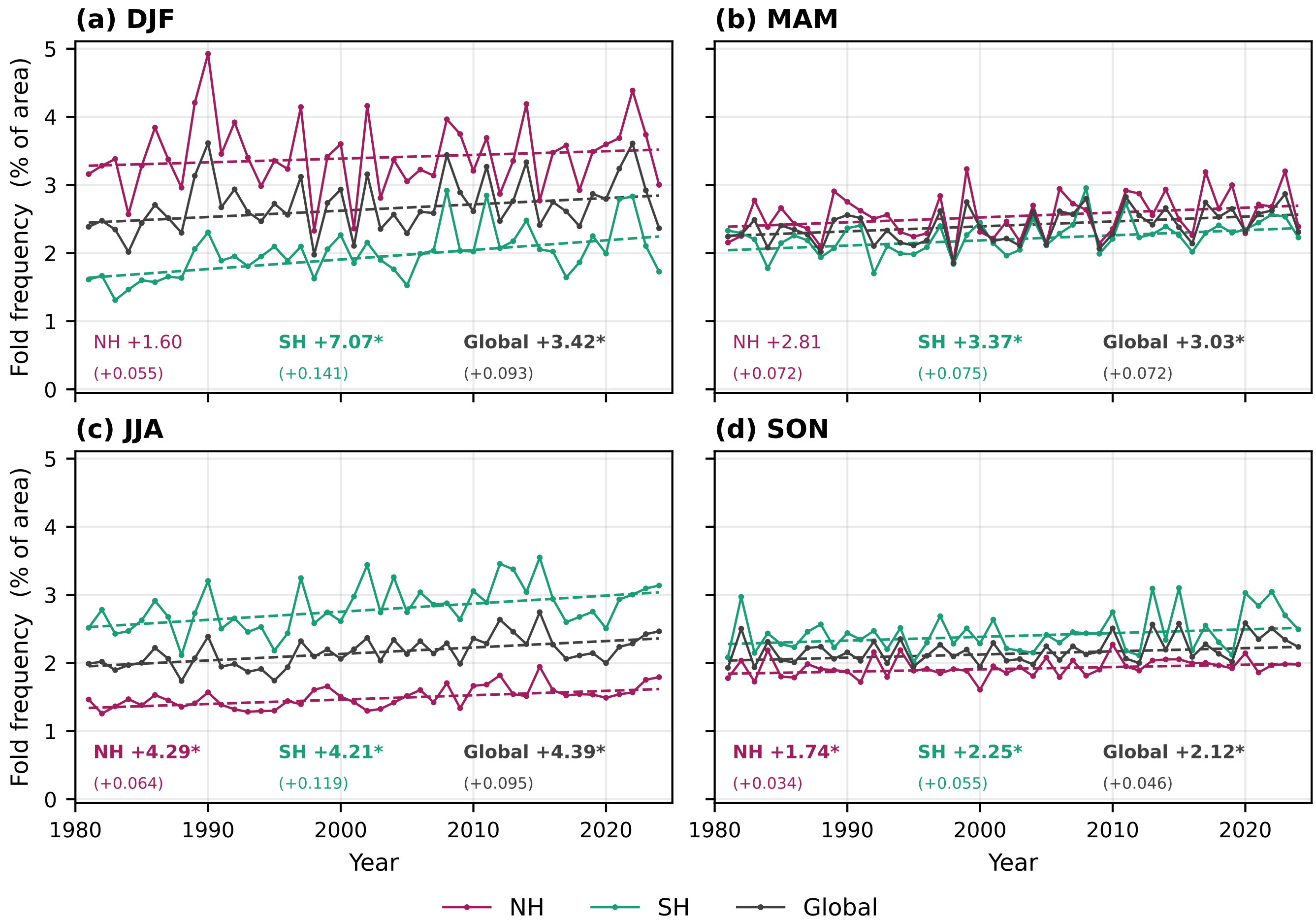


**Figure 12.** Seasonal mean TF frequency (solid) and Theil–Sen trend lines (dashed) over 1981–2024 for (a) DJF, (b) MAM, (c) JJA, and (d) SON, shown for the globe, NH, and SH (see legend). Frequency is the cosine-latitude weighted mean over $|\phi| \geq 10°$, expressed as a percentage of the corresponding reference area. Legend values give the trend as percent change per decade relative to the 1981–2024 mean; values in parentheses give the trend in the frequency itself (% of area per decade). Slopes significant at $\alpha_{\mathrm{FDR}} = 0.10$ after Benjamini–Hochberg FDR control over the four seasons of each region are shown in bold with an asterisk.

https://doi.org/10.5194/egusphere-2026-5480
Preprint. Discussion started: 23 September 2026


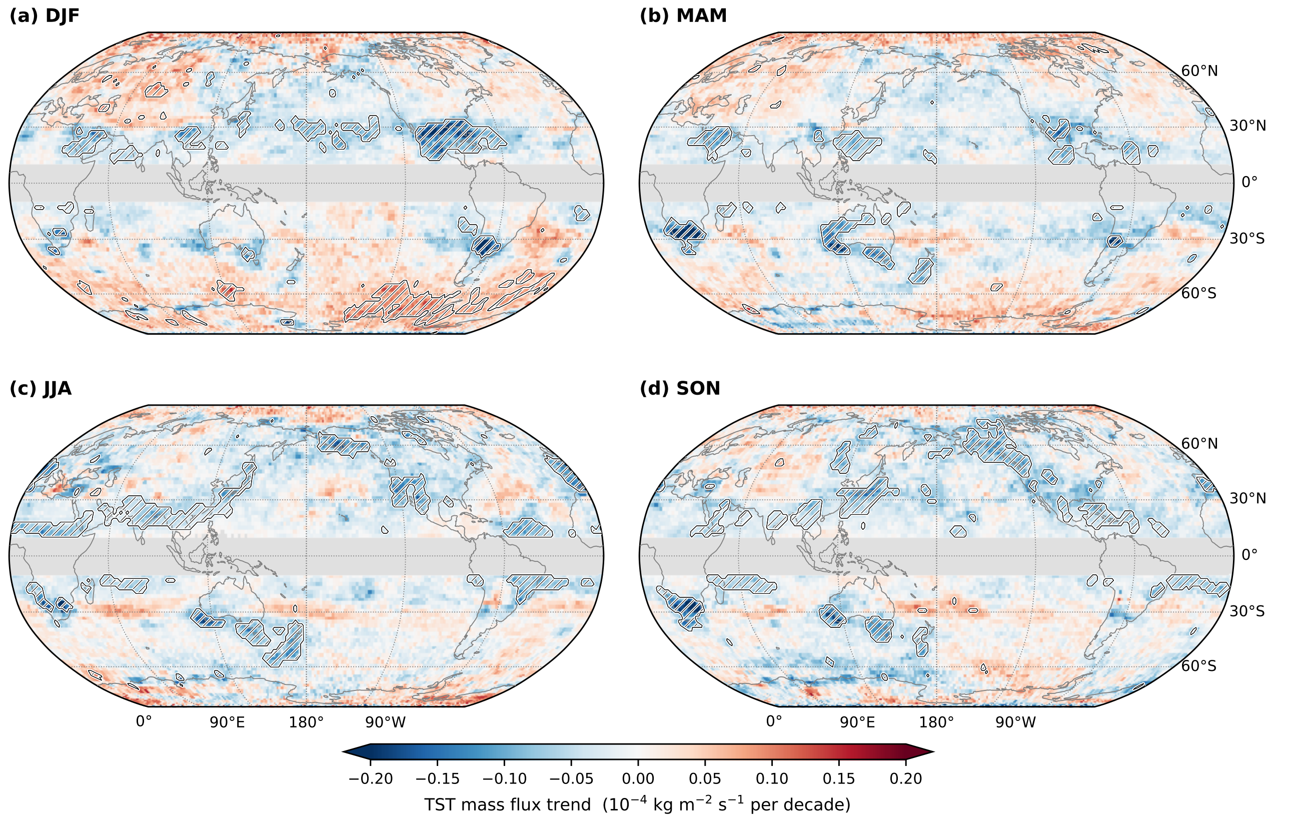


**Figure 13.** Trends of the seasonal mean TST mass flux over 1981–2024 (colors, in $10^{-4}\,\mathrm{kg\,m^{-2}\,s^{-1}}$ per decade) for (a) DJF, (b) MAM, (c) JJA, and (d) SON, on the 2° grid of Figure 3; grid boxes with non-zero flux in fewer than 40 of the 44 years are excluded. Hatched regions pass the Benjamini–Hochberg FDR criterion at $\alpha_{\mathrm{FDR}} = 0.10$.

is established that the chance of finding STT/TST events within roughly 250 km of a fold is greater than chance. Temporally, the mode of time lag between an air parcel's closest encounter to a TF and its crossing time is $-3$ h (parcel comes close to a TF grid box 3 h prior to crossing), which matches the physical expectation that folds facilitate the parcel or the surrounding environment for transport prior to the actual crossing event.

To objectively quantify each transport event's degree of association to TFs, the local false discovery rate is used. This framework allows us to assign a weight between zero and unity representing its likelihood of being TF associated. This method is objective in the sense that one does not need to choose collocation criteria (such as spatial separation thresholds), and there are no tunable parameters. However, its correctness relies on the validity of the null distribution. In this study, we built the null distribution by assessing the crossing-to-TF spatial relationship under the scenario that they have no relationship to each other but still possess their own seasonality. This is done by comparing a trajectory to the TF map from the same time of different

https://doi.org/10.5194/egusphere-2026-5480
Preprint. Discussion started: 23 September 2026


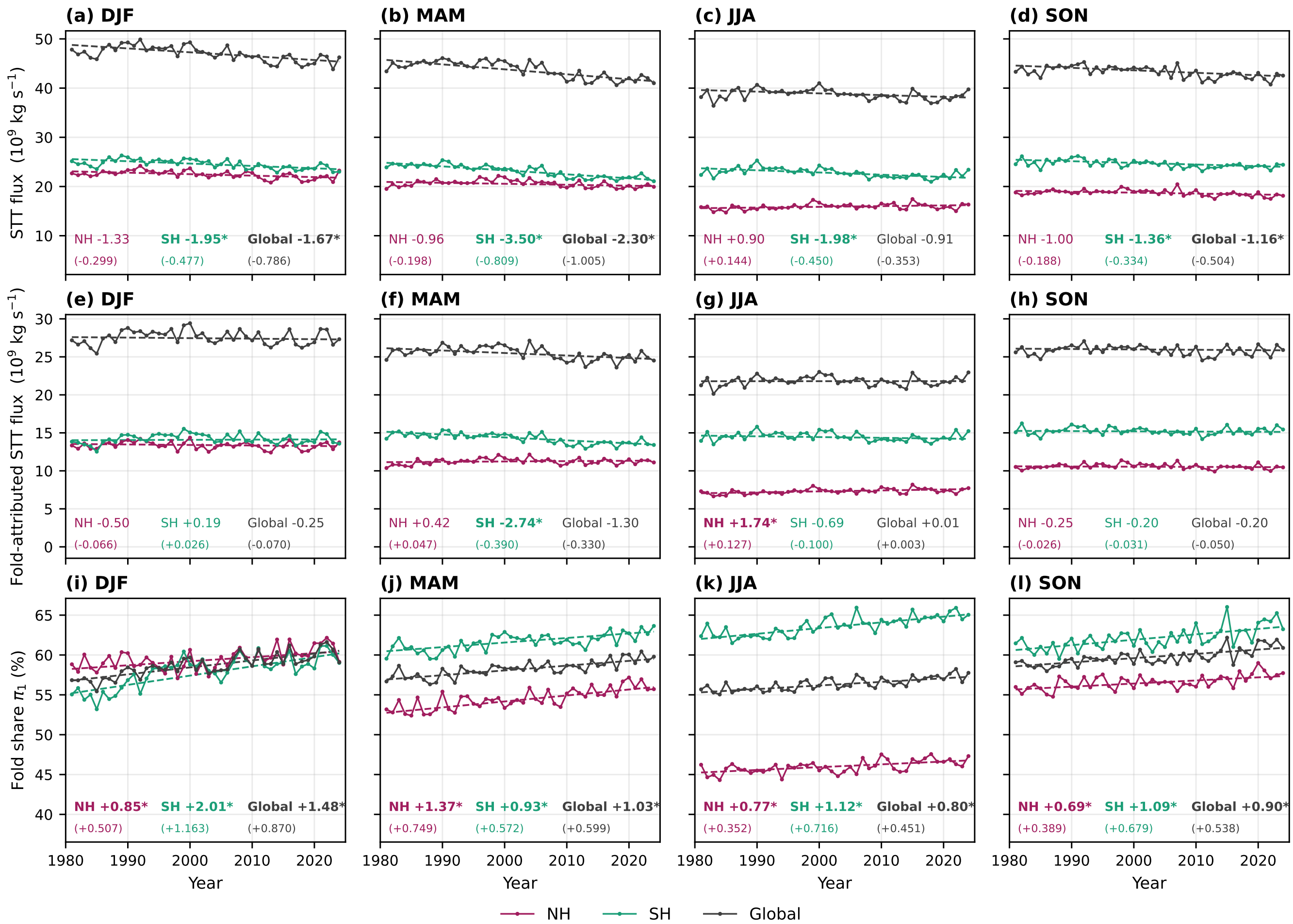


**Figure 14.** Seasonal mean STT mass flux (solid) and Theil–Sen trend lines (dashed) over 1981–2024 for the globe, NH, and SH (see legend). Rows show (a)–(d) the total STT flux, (e)–(h) the TF-associated STT flux, and (i)–(l) the TF-associated share, for DJF, MAM, JJA, and SON respectively. Fluxes are integrated over $|\phi| \geq 10^\circ$ (NH and SH denote $10^\circ$–$90^\circ$ N and S; global is their sum), and the TF-associated flux is the sum of $w(d_c, \phi_c)\,\Delta m$ over all crossings following Equation 7. The share in (i)–(l) is the ratio of the second row to the first. Legend values give the trend as percent change per decade relative to the 1981–2024 mean; values in parentheses give the trend in the units of the plotted quantity itself, i.e. $10^9\,\mathrm{kg\,s^{-1}}$ per decade in (a)–(h) and percentage points per decade in (i)–(l). Slopes significant at $\alpha_{\mathrm{FDR}} = 0.10$ after Benjamini–Hochberg FDR control over the eight season–direction tests of each region are shown in bold with an asterisk.

https://doi.org/10.5194/egusphere-2026-5480
Preprint. Discussion started: 23 September 2026


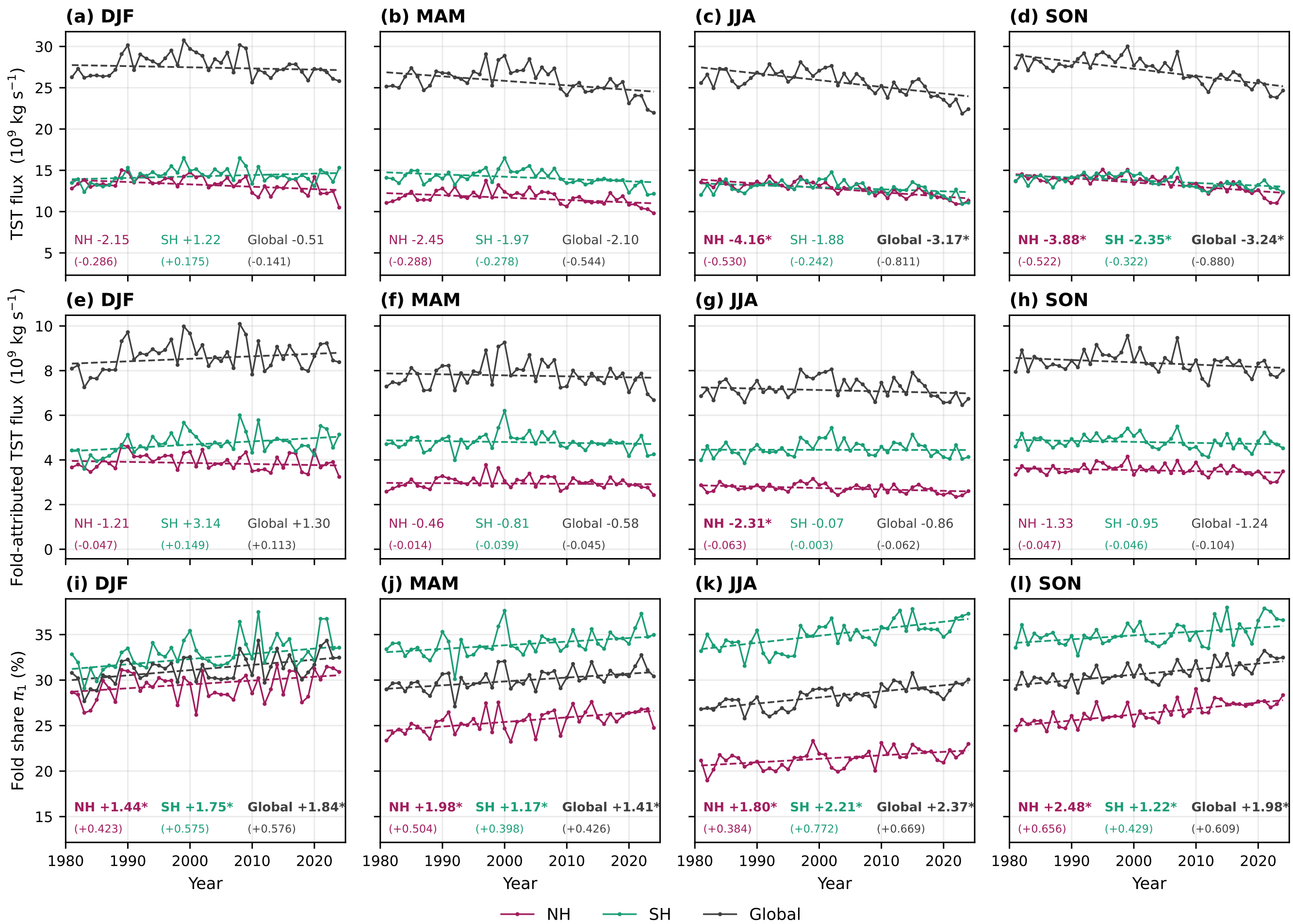


**Figure 15.** Same as Figure 14 except for TST.

years. One of the possible ways of testing this method's robustness may be to test different ways of constructing the null, though we have not conceived other ways that may improve upon the current method.

The main findings of this work are as follows:

1. Using the local fdr framework, the fraction of fold-associated transport $\hat{\pi}_1 = 1 - \hat{\pi}_0$, as shown in Figure 8 b and d, is highest generally in the subtropics. This echoes the findings of Sprenger et al. (2003) who also assessed the relationship of cross-tropopause exchange and TFs, arguing that TFs are a key feature of transport in the subtropics.

2. Over 1981–2024, TFs had increased in the SH and globally in all seasons. In the NH, statistically significant positive trends are found in JJA and SON. In seasonal maps of TF trends, most significant trends are positive and are localized mostly in high latitudes.

https://doi.org/10.5194/egusphere-2026-5480
Preprint. Discussion started: 23 September 2026


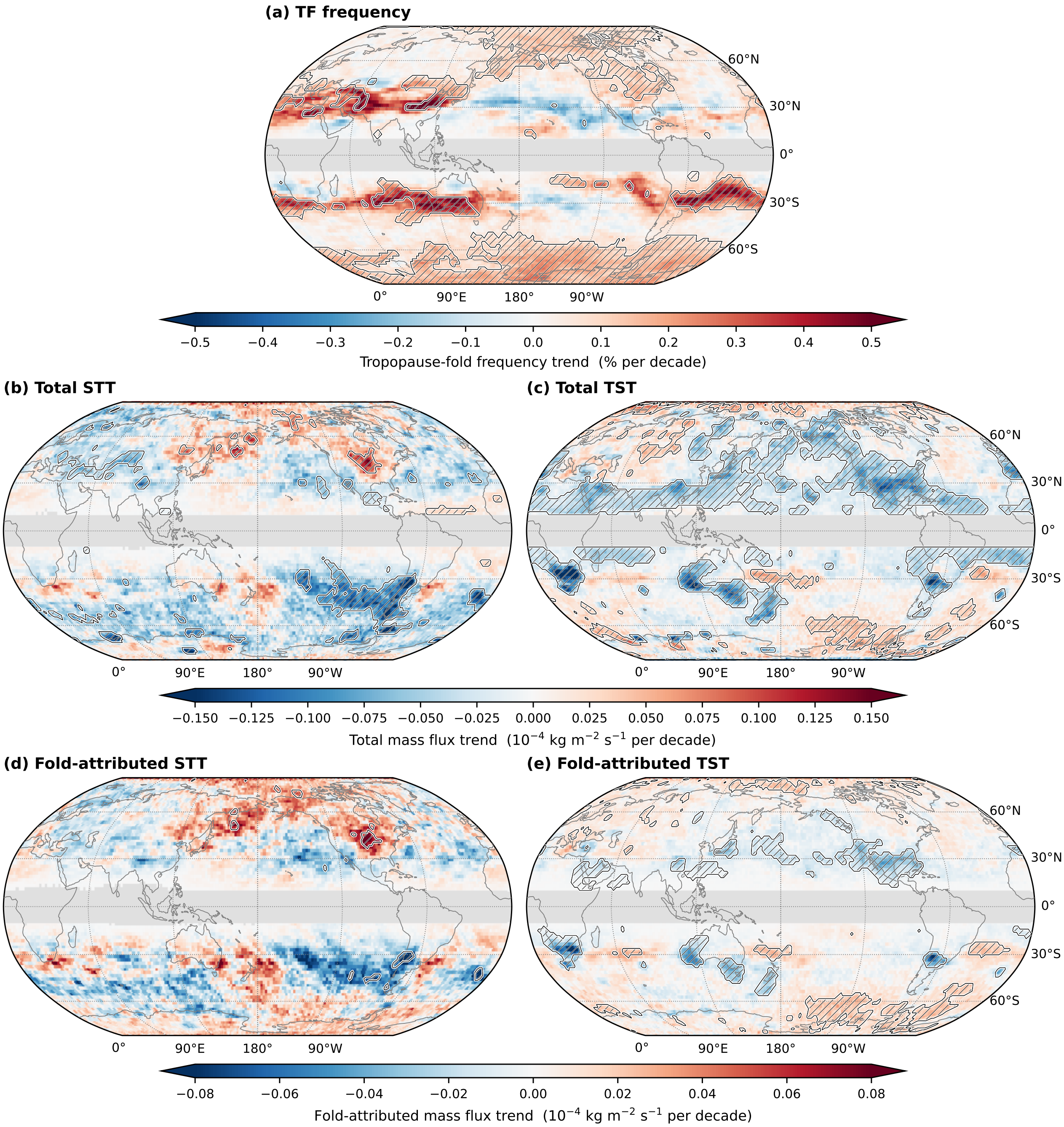


**Figure 16.** Trends of the annual mean over 1981–2024 for (a) TF frequency (% per decade), (b) total STT, (c) total TST, (d) TF-associated STT, and (e) TF-associated TST mass flux ($10^{-4}\,\mathrm{kg\,m^{-2}\,s^{-1}}$ per decade). Slopes are from the Theil–Sen estimator; hatching marks grid-points passing the Benjamini–Hochberg FDR criterion at $\alpha_{\mathrm{FDR}} = 0.10$.

https://doi.org/10.5194/egusphere-2026-5480
Preprint. Discussion started: 23 September 2026


3. Maps of seasonal STT fluxes practically exhibit no significant trends, while those of TST show numerous areas of significant negative trends.

4. Over 1981–2024, STT had decreased in the SH in all seasons; globally it decreased in all seasons except JJA. The fold-attributed STT is relatively flat (showing very few significant trends), but the fold share had increased in all seasons and both hemispheres as well as globally. This suggests that the decrease in STT is accounted for by transport not related to folds.

5. Over the study period, global and NH TST decreased during JJA and SON, while trends in fold-attributed TST are generally not significant (similar to STT). Fold share of TST also had increased in all seasons and both hemispheres and globally. Like STT, this implies that the TST decrease is occurring in transport unrelated to folds.

6. Globally, TFs are estimated to be associated with 58.3% (30.1%) of STT (TST) fluxes. STT is evidently more associated with folds than TST.

7. Assuming the validity of the null distribution, the estimated fold-attributed fractions represent a lower bound. This is because as Equation 6 shows, the minimum of $r(d)$ serves as an upper bound of $\pi_0$. As a result, the estimated nonnull fractions $\hat{\pi}_1$ represent a lower bound.

Though folds are thought to be one of the dominant mechanisms of STT, our results suggest there is more than 40% of it that is not accounted for by folds. A meaningful direction for future work would be to elucidate the processes responsible for the non-fold transport. Also, spatial patterns of STT and TST show general agreement across studies employing the Lagrangian method, but many of their features have not been explained in detail: the STT maxima over Asia during MAM and JJA, which may be related to the upper-tropospheric anticyclones; the STT and TST hotspot near the Andes; and the tendency toward greater STT and TST in the SH.

*Data availability.* The ERA5 reanalysis is available from the Copernicus Data store (https://cds.climate.copernicus.eu/).

*Author contributions.* K.-W. Chang conceived the core ideas (scientific question and local fdr) and wrote the code for the Lagrangian transport, while C.-H. Chung performed calculations to produce the fold, STT, and TST climatolgies and trends. Both authors contributed to plotting and writing.

*Competing interests.* The authors declare that there are no competing interests.

https://doi.org/10.5194/egusphere-2026-5480
Preprint. Discussion started: 23 September 2026


*Acknowledgements.* This study was funded by the National Science and Technology Council (NSTC) under grant 111-2111-M-034-004-MY3 and 114-2111-M-034-003. We thank Kenneth P. Bowman for providing the TRAJ3D model and helpful discussions. GNU parallel (Tange, 2018) was used in this study. Artificial intelligence (AI) coding tools were used in assisting the development of code for calculating the results and plotting, as well as proofreading of the manuscript.

https://doi.org/10.5194/egusphere-2026-5480
Preprint. Discussion started: 23 September 2026


## References

Abalos, M., Orbe, C., Kinnison, D. E., Plummer, D., Oman, L. D., Jöckel, P., Morgenstern, O., Garcia, R. R., Zeng, G., Stone, K. A., and Dameris, M.: Future Trends in Stratosphere-to-Troposphere Transport in CCMI Models, Atmospheric Chemistry and Physics, 20, 6883–6901, https://doi.org/10.5194/acp-20-6883-2020, 2020.

Akritidis, D., Pozzer, A., Zanis, P., Tyrlis, E., Škerlak, B., Sprenger, M., and Lelieveld, J.: On the Role of Tropopause Folds in Summertime Tropospheric Ozone over the Eastern Mediterranean and the Middle East, Atmospheric Chemistry and Physics, 16, 14 025–14 039, https://doi.org/10.5194/acp-16-14025-2016, 2016.

Akritidis, D., Katragkou, E., Zanis, P., Pytharoulis, I., Melas, D., Flemming, J., Inness, A., Clark, H., Plu, M., and Eskes, H.: A Deep Stratosphere-to-Troposphere Ozone Transport Event over Europe Simulated in CAMS Global and Regional Forecast Systems: Analysis and Evaluation, Atmospheric Chemistry and Physics, 18, 15 515–15 534, https://doi.org/10.5194/acp-18-15515-2018, 2018.

Austin, J. F. and Midgley, R. P.: The Climatology of the Jet Stream and Stratospheric Intrusions of Ozone over Japan, Atmospheric Environment, 28, 39–52, https://doi.org/10.1016/1352-2310(94)90021-3, 1994.

Benjamini, Y. and Hochberg, Y.: Controlling the False Discovery Rate: A Practical and Powerful Approach to Multiple Testing, Journal of the Royal Statistical Society Series B: Statistical Methodology, 57, 289–300, https://doi.org/10.1111/j.2517-6161.1995.tb02031.x, 1995.

Bourqui, M.: Analysis and Quantification of STE: A Novel Approach, https://doi.org/10.3929/ethz-a-004184420, 2001.

Bourqui, M. S.: Stratosphere-Troposphere Exchange from the Lagrangian Perspective: A Case Study and Method Sensitivities, Atmospheric Chemistry and Physics, 6, 2651–2670, https://doi.org/10.5194/acp-6-2651-2006, 2006.

Bourqui, M. S. and Trpanier, P. Y.: Descent of Deep Stratospheric Intrusions during the IONS August 2006 Campaign, Journal of Geophysical Research Atmospheres, 115, 1–16, https://doi.org/10.1029/2009JD013183, 2010.

Bowman, K. P.: Large-Scale Isentropic Mixing Properties of the Antarctic Polar Vortex from Analyzed Winds, Journal of Geophysical Research, 98, 23 013–23 013, https://doi.org/10.1029/93JD02599, 1993.

Chang, K.-W., Bowman, K. P., Siu, L. W., and Rapp, A. D.: Convective Forcing of the North American Monsoon Anticyclone at Intraseasonal and Interannual Time Scales, Journal of the Atmospheric Sciences, 78, 2941–2956, https://doi.org/10.1175/JAS-D-21-0009.1, 2021.

Clapp, C. E., Smith, J. B., Bedka, K. M., and Anderson, J. G.: Identifying Outflow Regions of North American Monsoon Anticyclone-Mediated Meridional Transport of Convectively Influenced Air Masses in the Lower Stratosphere, Journal of Geophysical Research: Atmospheres, 126, 1–19, https://doi.org/10.1029/2021JD034644, 2021.

Ding, A. and Wang, T.: Influence of Stratosphere-to-troposphere Exchange on the Seasonal Cycle of Surface Ozone at Mount Waliguan in Western China, Geophysical Research Letters, 33, https://doi.org/10.1029/2005GL024760, 2006.

Dunkerton, T. J.: Evidence of Meridional Motion in the Summer Lower Stratosphere Adjacent to Monsoon Regions, Journal of Geophysical Research, 100, 16 675–16 675, https://doi.org/10.1029/95JD01263, 1995.

Efron, B.: Microarrays, Empirical Bayes and the Two-Groups Model, Statistical Science, 23, https://doi.org/10.1214/07-STS236, 2008.

Fabian, P. and Pruchniewicz, P. G.: Meridional Distribution of Ozone in the Troposphere and Its Seasonal Variations, Journal of Geophysical Research, 82, 2063–2073, https://doi.org/10.1029/JC082i015p02063, 1977.

Galani, E., Balis, D., Zanis, P., Zerefos, C., Papayannis, A., Wernli, H., and Gerasopoulos, E.: Observations of Stratosphere-to-troposphere Transport Events over the Eastern Mediterranean Using a Ground-based Lidar System, Journal of Geophysical Research: Atmospheres, 108, https://doi.org/10.1029/2002JD002596, 2003.

Gettelman, A. and Sobel, A. H.: Direct Diagnoses of Stratosphere-Troposphere Exchange, Tech. Rep. 1, 2000.

https://doi.org/10.5194/egusphere-2026-5480
Preprint. Discussion started: 23 September 2026


Gray, S. L.: Mechanisms of Midlatitude Cross-tropopause Transport Using a Potential Vorticity Budget Approach, Journal of Geophysical Research: Atmospheres, 111, https://doi.org/10.1029/2005JD006259, 2006.

Hersbach, H., Bell, B., Berrisford, P., Hirahara, S., Horányi, A., Muñoz-Sabater, J., Nicolas, J., Peubey, C., Radu, R., Schepers, D., Simmons, A., Soci, C., Abdalla, S., Abellan, X., Balsamo, G., Bechtold, P., Biavati, G., Bidlot, J., Bonavita, M., De Chiara, G., Dahlgren, P., Dee, D., Diamantakis, M., Dragani, R., Flemming, J., Forbes, R., Fuentes, M., Geer, A., Haimberger, L., Healy, S., Hogan, R. J., Hólm, E., Janisková, M., Keeley, S., Laloyaux, P., Lopez, P., Lupu, C., Radnoti, G., De Rosnay, P., Rozum, I., Vamborg, F., Villaume, S., and Thépaut, J.-N.: The ERA5 Global Reanalysis, Quarterly Journal of the Royal Meteorological Society, 146, 1999–2049, https://doi.org/10.1002/qj.3803, 2020.

Hoerling, M. P., Schaack, T. K., and Lenzen, A. J.: A Global Analysis of Stratospheric–Tropospheric Exchange during Northern Winter, Monthly Weather Review, 121, 162–172, https://doi.org/10.1175/1520-0493(1993)121<0162:AGAOSE>2.0.CO;2, 1993.

Holton, J. R., Haynes, P. H., McIntyre, M. E., Douglass, A. R., Rood, R. B., and Pfister, L.: Stratosphere-Troposphere Exchange, Reviews of Geophysics, 33, 403–403, https://doi.org/10.1029/95RG02097, 1995.

Hoskins, B. J. and Hodges, K. I.: A New Perspective on Southern Hemisphere Storm Tracks, Journal of Climate, 18, 4108–4129, https://doi.org/10.1175/JCLI3570.1, 2005.

Hoskins, B. J. and Rodwell, M. J.: A Model of the Asian Summer Monsoon. Part I: The Global Scale, Journal of the Atmospheric Sciences, 52, 1329–1340, https://doi.org/10.1175/1520-0469(1995)052<1329:AMOTAS>2.0.CO;2, 1995.

James, P., Stohl, A., Forster, C., Eckhardt, S., Seibert, P., and Frank, A.: A 15-Year Climatology of Stratosphere-Troposphere Exchange with a Lagrangian Particle Dispersion Model: 2. Mean Climate and Seasonal Variability, Journal of Geophysical Research Atmospheres, 108, 1–16, https://doi.org/10.1029/2002jd002639, 2003.

Kendall, M. G.: Rank Correlation Methods, Griffin, London, 4. ed., 2. impr edn., ISBN 978-0-85264-199-6, 1975.

Knowland, K. E., Ott, L. E., Duncan, B. N., and Wargan, K.: Stratospheric Intrusion-Influenced Ozone Air Quality Exceedances Investigated in the NASA MERRA-2 Reanalysis, Geophysical Research Letters, 44, 10,691–10,701, https://doi.org/10.1002/2017GL074532, 2017.

Kuang, S., Newchurch, M. J., Burris, J., Wang, L., Knupp, K., and Huang, G.: Stratosphere-to-Troposphere Transport Revealed by Ground-Based Lidar and Ozonesonde at a Midlatitude Site, Journal of Geophysical Research Atmospheres, 117, https://doi.org/10.1029/2012JD017695, 2012.

Kuang, S., Newchurch, M. J., Johnson, M. S., Wang, L., Burris, J., Pierce, R. B., Eloranta, E. W., Pollack, I. B., Graus, M., de Gouw, J., Warneke, C., Ryerson, T. B., Markovic, M. Z., Holloway, J. S., Pour-Biazar, A., Huang, G., Liu, X., and Feng, N.: Summertime Tropospheric Ozone Enhancement Associated with a Cold Front Passage Due to Stratosphere-Totroposphere Transport and Biomass Burning: Simultaneous Ground-Based Lidar and Airborne Measurements, Journal of Geophysical Research, 122, 1293–1311, https://doi.org/10.1002/2016JD026078, 2017.

Kumar, K. N., Sharma, S. K., Naja, M., and Phanikumar, D. V.: A Rossby Wave Breaking-Induced Enhancement in the Tropospheric Ozone over the Central Himalayan Region, Atmospheric Environment, 224, 117 356–117 356, https://doi.org/10.1016/j.atmosenv.2020.117356, 2020.

Kunsch, H. R.: The Jackknife and the Bootstrap for General Stationary Observations, The Annals of Statistics, 17, https://doi.org/10.1214/aos/1176347265, 1989.

Lamarque, J.-F. and Hess, P. G.: Cross-Tropopause Mass Exchange and Potential Vorticity Budget in a Simulated Tropopause Folding, Journal of the Atmospheric Sciences, 51, 2246–2269, https://doi.org/10.1175/1520-0469(1994)051<2246:ctmeap>2.0.co;2, 1994.

https://doi.org/10.5194/egusphere-2026-5480
Preprint. Discussion started: 23 September 2026


Langford, A. O., Aikin, K. C., Eubank, C. S., and Williams, E. J.: Stratospheric Contribution to High Surface Ozone in Colorado during Springtime, Geophysical Research Letters, 36, https://doi.org/10.1029/2009GL038367, 2009.

Langford, A. O., Brioude, J., Cooper, O. R., Senff, C. J., Alvarez, R. J., Hardesty, R. M., Johnson, B. J., and Oltmans, S. J.: Stratospheric Influence on Surface Ozone in the Los Angeles Area during Late Spring and Early Summer of 2010, Journal of Geophysical Research Atmospheres, 117, https://doi.org/10.1029/2011JD016766, 2012.

Langford, A. O., Alvarez, R. J., Brioude, J., Evan, S., Iraci, L. T., Kirgis, G., Kuang, S., Leblanc, T., Newchurch, M. J., Pierce, R. B., Senff, C. J., and Yates, E. L.: Coordinated Profiling of Stratospheric Intrusions and Transported Pollution by the Tropospheric Ozone Lidar Network (TOLNet) and NASA Alpha Jet Experiment (AJAX): Observations and Comparison to HYSPLIT, RAQMS, and FLEXPART, Atmospheric Environment, 174, 1–14, https://doi.org/10.1016/j.atmosenv.2017.11.031, 2018.

Lin, M., Fiore, A. M., Horowitz, L. W., Langford, A. O., Oltmans, S. J., Tarasick, D., and Rieder, H. E.: Climate Variability Modulates Western US Ozone Air Quality in Spring via Deep Stratospheric Intrusions, pp. 1–11, https://doi.org/10.1038/ncomms81, 2015.

Lin, Y., Tian, W., Xue, H., Luo, J., Zhang, J., Tian, H., and Liang, W.: Global Trends of Tropopause Folds in Recent Decades, Atmospheric and Oceanic Science Letters, 17, 100 450–100 450, https://doi.org/10.1016/j.aosl.2023.100450, 2024.

Liu, J., Rodriguez, J. M., Thompson, A. M., Logan, J. A., Douglass, A. R., Olsen, M. A., Steenrod, S. D., and Posny, F.: Origins of Tropospheric Ozone Interannual Variation over Réunion: A Model Investigation, Journal of Geophysical Research, 121, 521–537, https://doi.org/10.1002/2015JD023981, 2016.

Luo, Y., Zhao, T., Meng, K., Hu, J., Yang, Q., Bai, Y., Yang, K., Fu, W., Tan, C., Zhang, Y., Zhang, Y., and Li, Z.: A Mechanism of Stratospheric O3 Intrusion into the Atmospheric Environment: A Case Study of the North China Plain, Atmospheric Chemistry and Physics, 24, 7013–7026, https://doi.org/10.5194/acp-24-7013-2024, 2024.

Mann, H. B.: Nonparametric Tests Against Trend, Econometrica, 13, 245–245, https://doi.org/10.2307/1907187, 1945.

Roelofs, G.-J. and Lelieveld, J.: Model Study of the Influence of Cross-Tropopause O3 Transports on Tropospheric O3 Levels, Tellus B: Chemical and Physical Meteorology, 49, 38–38, https://doi.org/10.3402/tellusb.v49i1.15949, 1997.

Sen, P. K.: Estimates of the Regression Coefficient Based on Kendall's Tau, Journal of the American Statistical Association, 63, 1379–1389, https://doi.org/10.1080/01621459.1968.10480934, 1968.

Seo, K. H. and Bowman, K. P.: Lagrangian Estimate of Global Stratosphere-Troposphere Mass Exchange, Journal of Geophysical Research Atmospheres, 107, ACL 2–8, https://doi.org/10.1029/2002JD002441, 2002.

Siegmund, P. C., van Velthoven, P. F. J., and Kelder, H.: Cross-tropopause Transport in the Extratropical Northern Winter Hemisphere, Diagnosed from High-resolution ECMWF Data, Quarterly Journal of the Royal Meteorological Society, 122, 1921–1941, https://doi.org/10.1002/qj.49712253609, 1996.

Siu, L. W. and Bowman, K. P.: Forcing of the Upper-Tropospheric Monsoon Anticyclones, Journal of the Atmospheric Sciences, 76, 1937–1954, https://doi.org/10.1175/JAS-D-18-0340.1, 2019.

Škerlak, B., Sprenger, M., and Wernli, H.: A Global Climatology of Stratosphere-Troposphere Exchange Using the ERA-Interim Data Set from 1979 to 2011, Atmospheric Chemistry and Physics, 14, 913–937, https://doi.org/10.5194/acp-14-913-2014, 2014.

Škerlak, B., Sprenger, M., Pfahl, S., Tyrlis, E., and Wernli, H.: Tropopause Folds in ERA-interim: Global Climatology and Relation to Extreme Weather Events, Journal of Geophysical Research, 120, 4860–4877, https://doi.org/10.1002/2014JD022787, 2015.

Spaete, P., Johnson, D. R., and Schaack, T. K.: Stratospheric–Tropospheric Mass Exchange during the Presidents' Day Storm, Monthly Weather Review, 122, 424–439, https://doi.org/10.1175/1520-0493(1994)122<0424:SMEDTP>2.0.CO;2, 1994.

https://doi.org/10.5194/egusphere-2026-5480
Preprint. Discussion started: 23 September 2026


Sprenger, M., Maspoli, M. C., and Wernli, H.: Tropopause Folds and Cross-Tropopause Exchange: A Global Investigation Based upon ECMWF Analyses for the Time Period March 2000 to February 2001, Journal of Geophysical Research Atmospheres, 108, https://doi.org/10.1029/2002jd002587, 2003.

Stohl, A., Bonasoni, P., Cristofanelli, P., Collins, W., Feichter, J., Frank, A., Forster, C., Gerasopoulos, E., Gäggeler, H., James, P., Kentarchos, T., Kromp-Kolb, H., Krüger, B., Land, C., Meloen, J., Papayannis, A., Priller, A., Seibert, P., Sprenger, M., Roelofs, G. J., Scheel, H. E., Schnabel, C., Siegmund, P., Tobler, L., Trickl, T., Wernli, H., Wirth, V., Zanis, P., and Zerefos, C.: Stratosphere-Troposphere Exchange: A Review, and What We Have Learned from STACCATO, Journal of Geophysical Research Atmospheres, 108, https://doi.org/10.1029/2002jd002490, 2003.

Tange, O.: GNU Parallel 2018, Isbn 9781387509881, Ole Tange, ISBN 978-1-387-50988-1, https://doi.org/10.5281/zenodo.1146014, 2018.

Thompson, A. M., Balashov, N. V., Witte, J. C., Coetzee, J. G., Thouret, V., and Posny, F.: Tropospheric Ozone Increases over the Southern Africa Region: Bellwether for Rapid Growth in Southern Hemisphere Pollution?, Atmospheric Chemistry and Physics, 14, 9855–9869, https://doi.org/10.5194/acp-14-9855-2014, 2014.

Trickl, T., Vogelmann, H., Fix, A., Schäfler, A., Wirth, M., Calpini, B., Levrat, G., Romanens, G., Apituley, A., Wilson, K. M., Begbie, R., Reichardt, J., Vömel, H., and Sprenger, M.: How Stratospheric Are Deep Stratospheric Intrusions? LUAMI 2008, Atmospheric Chemistry and Physics, 16, 8791–8815, https://doi.org/10.5194/acp-16-8791-2016, 2016.

Tyrlis, E., Škerlak, B., Sprenger, M., Wernli, H., Zittis, G., and Lelieveld, J.: On the Linkage between the Asian Summer Monsoon and Tropopause Fold Activity over the Eastern Mediterranean and the Middle East, Journal of Geophysical Research: Atmospheres, 119, 3202–3221, https://doi.org/10.1002/2013JD021113, 2014.

Wei, M.-Y.: A New Formulation of the Exchange of Mass and Trace Constituents between the Stratosphere and Troposphere, Journal of the Atmospheric Sciences, 44, 3079–3086, https://doi.org/10.1175/1520-0469(1987)044<3079:ANFOTE>2.0.CO;2, 1987.

Wernli, H. and Bourqui, M.: A Lagrangian "1-Year Climatology" of (Deep) Cross-Tropopause Exchange in the Extratropical Northern Hemisphere, Journal of Geophysical Research Atmospheres, 107, https://doi.org/10.1029/2001jd000812, 2002.

Wilks, D. S.: Resampling Hypothesis Tests for Autocorrelated Fields, Journal of Climate, 10, 65–82, https://doi.org/10.1175/1520-0442(1997)010<0065:RHTFAF>2.0.CO;2, 1997.

Wilks, D. S.: “The Stippling Shows Statistically Significant Grid Points”: How Research Results Are Routinely Overstated and Overinterpreted, and What to Do about It, Bulletin of the American Meteorological Society, 97, 2263–2273, https://doi.org/10.1175/BAMS-D-15-00267.1, 2016.

Wirth, V.: Diabatic Heating in an Axisymmetric Cut-off Cyclone and Related Stratosphere-troposphere Exchange, Quarterly Journal of the Royal Meteorological Society, 121, 127–147, https://doi.org/10.1002/qj.49712152107, 1995.

Wirth, V. and Egger, J.: Diagnosing Extratropical Synoptic-scale Stratosphere-troposphere Exchange: A Case Study, Quarterly Journal of the Royal Meteorological Society, 125, 635–655, https://doi.org/10.1002/qj.49712555413, 1999.

Wu, Y., Chen, G., Taylor, L., and Zhang, P.: On the Linkage Between the Asian Summer Monsoon and Tropopause Folds, Journal of Geophysical Research: Atmospheres, 123, 2037–2049, https://doi.org/10.1002/2017JD027870, 2018.

Yan, X., Konopka, P., Ploeger, F., Podglajen, A., Wright, J. S., Müller, R., and Riese, M.: The Efficiency of Transport into the Stratosphere via the Asian and North American Summer Monsoon Circulations, Atmospheric Chemistry and Physics, 19, 15 629–15 649, https://doi.org/10.5194/acp-19-15629-2019, 2019.

Zanis, P., Hadjinicolaou, P., Pozzer, A., Tyrlis, E., Dafka, S., Mihalopoulos, N., and Lelieveld, J.: Summertime Free-Tropospheric Ozone Pool over the Eastern Mediterranean/Middle East, Atmospheric Chemistry and Physics, 14, 115–132, https://doi.org/10.5194/acp-14-115-2014, 2014.

Zhang, J., Gong, X., Crosbie, E., Diskin, G., Froyd, K., Hall, S., Kupc, A., Moore, R., Peischl, J., Rollins, A., Schwarz, J., Shook, M., Thompson, C., Ullmann, K., Williamson, C., Wisthaler, A., Xu, L., Ziemba, L., Brock, C. A., and Wang, J.: Stratospheric Air Intrusions Promote Global-Scale New Particle Formation, Science, 385, 210–216, https://doi.org/10.1126/science.adn2961, 2024.

Zhang, L., Jacob, D. J., Yue, X., Downey, N. V., Wood, D. A., and Blewitt, D.: Sources Contributing to Background Surface Ozone in the US Intermountain West, Atmospheric Chemistry and Physics, 14, 5295–5309, https://doi.org/10.5194/acp-14-5295-2014, 2014.